SEMARAK ILMU PUBLISHING

Journal of Advanced Research in Fluid Mechanics and Thermal Sciences

Journal homepage:
https://semarakilmu.com.my/journals/index.php/fluid_mechanics_thermal_sciences/index
ISSN: 2289-7879

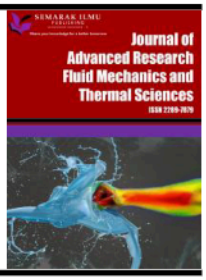

Passive Control of Base Drag with D-Shaped Rib in a Suddenly Expanded Flow

Newaz Md Ashif[1], Abdul Aabid[2], Mohd. Azan Mohammad Sapardi[1], S. M. Afzal Hoq[3], Sher Afghan Khan[1,*], Khizar Ahmed Pathan[4]

[1] Department of Mechanical & Aerospace Engineering, Faculty of Engineering, IIUM, Kuala Lumpur, Malaysia
[2] Prince Sultan University, Riyadh, Saudi Arabia
[3] Department of Science, Faculty of Engineering, IIUM, Kuala Lumpur, Malaysia
[4] Department of Mechanical Engineering, CSMSS Chh. Shahu College of Engineering, Aurangabad 431011, Maharashtra, India

ARTICLE INFO

Article history:
Received 17 March 2025
Received in revised form 15 June 2025
Accepted 23 June 2025
Available online 15 July 2025

Keywords:
D-shaped rib; base drag; Mach number; rib location; L/D ratio

ABSTRACT

The sudden increase in area at the blunt base of rockets, missiles, projectiles, and automobiles is widespread. The sudden rise in the base area leads to flow separation and reattachment, and the pressure in the separated recirculation zone is lower than the ambient pressure. In this study, a passive control in the form of a D-shaped rib is suggested to control the base pressure and, hence, the base drag, which is considerable at the critical Mach numbers. The present study aims to regulate the base pressure using D-shaped ribs of various heights and radii at sonic Mach numbers. The duct diameter and length-to-diameter (L/D) ratios were from 1 to 6, and rib locations were considered at L/D = 0.5, 1, 1.5, 2, and 3. When the rib has orientation 2, and the shear layer faces the straight part of the rib, the base pressure's magnitude is higher than in orientation 1. It is seen that with a 1 mm rib as a control mechanism, the base pressure attains a value more than ambient pressure. Hence, if the user must equate the base pressure with atmospheric pressure, then a 1 mm rib radius at L/D = 1 is the right choice. If it is required to raise the base pressure by a considerable value, then higher values of rib radius are to be considered.

1. Introduction

Turbulence has been a mystery since the beginning of fluid science research. Since practically all engineering and natural processes around us are turbulent and cannot be avoided, we must understand turbulence. Drag is related to turbulent flows, and drag control requires understanding the turbulence. Turbulence is required in some flows, such as when fluids are mixed. However, turbulence is undesirable and should be controlled in engineering flows where energy input is to be minimized. Turbulent drag has significant financial and environmental impacts on engineering and real-world flows, primarily due to the combustion by-products and the fossil fuels used by various forms of transportation, which account for more than 20% of overall emissions [1].

* *Corresponding author.*
E-mail address: sakhan@iium.edu.my

https://doi.org/10.37934/arfmts.133.2.4376

In subsonic and supersonic regimes, sudden flow expansion is a significant issue with numerous applications. A great way to solve sudden expansion problems is to employ a jet and a shroud arrangement as a supersonic parallel diffuser. The system that simulates high altitude conditions in test cells for jet engines and rocket engines has another intriguing use: a jet discharging into a shroud and creating a sufficient sub-atmospheric discharge pressure. An internal combustion engine's exhaust port has a similar flow state; a jet of hot exhaust gases travels through the exhaust valve. The flow around the base of a projectile or missile in flight with a blunt edge is another pertinent example, where the flow expands inward rather than outward, as in the preceding case.

Flow separation, recirculation, and reattachment are characteristics of the complicated phenomena known as the flow field of abrupt axisymmetric expansion. As shown in Figure 1, a dividing streamline (dividing surface) may split such a flow field into two core regions: the central and recirculation regions. The reattachment point is the location where the dividing streamline meets the wall. The length between the base and the reattachment point is called the reattachment length. The reattachment length is a strong function of the Mach number at the nozzle exit, the enlarged duct area, and the expansion level. The reattachment length will vary based on the expansion level and the base pressure value.

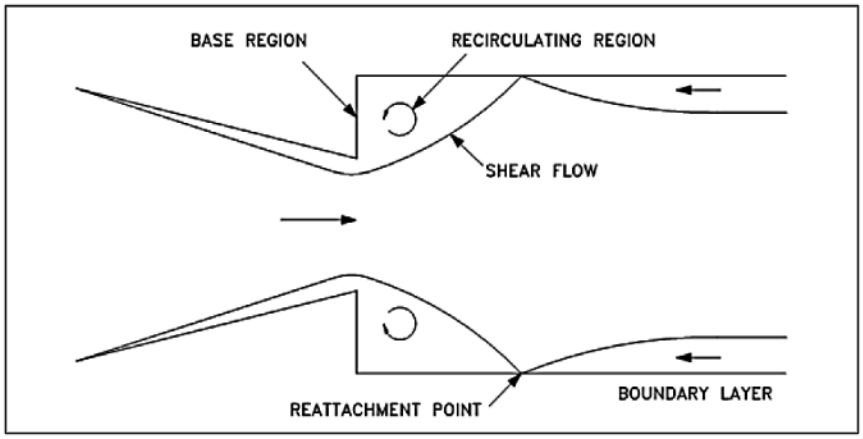

Fig. 1. Converging diverging nozzle (a) A view of the flow field from the converging nozzle and duct at Sonic Mach number (b) The flow field when the nozzle is under-expanded at Sonic Mach number

It would be preferable to understand the physics of the flow when the shear layer is exhausted in a duct with a larger area before examining the base pressure data. The boundary layer will detach, expand, and rejoin the duct after leaving the nozzle when the Mach number is less than unity. Since the first vortex is near the base and relatively robust, the separated region will have one or more vortices. The central vortex is the name given to this vortex. It will function as a pump, moving fluids from the base area to the main jet on the boundary layer's edge. Due to this pushing activity, low pressure will result in the recirculation zone. Pushing action is too sporadic because this vortex spread is known to occur periodically. The base pressure fluctuates as a result of this erratic pattern. These changes in the base pressure, however, are shown to be insignificant during the testing process. To analyze the results, we thus use the mean base pressure values. The cyclicity of the vortex desquamation may cause the entire flow pattern of the duct to oscillate. For geometrical and inertia values, these oscillations could become highly severe. The degree of expansion, reattachment length, Mach number, and area ratio are the primary determinants of the intensity of the central vortex at the base.

2. Literature Review

The aerodynamic shape is necessary for reducing drag and improving efficiency in engineering applications. Khan *et al.,* [1] conducted a CFD analysis of a human-powered submarine to study drag reduction. They found that the streamlined designs reduce the drag by reducing flow separation. This study gives the role of geometric changes in managing aerodynamic drag [1]. Pathan *et al.,* [2] studied the influence of a boat-tail helmet on drag reduction. They found that the changes in the shape significantly change flow patterns and pressure distribution, leading to lower drag. Their findings support using passive control techniques for aerodynamic improvements [2]. Pathan *et al.,* [2] explored thrust and base pressure parameters in suddenly expanded flows. They found that the nozzle pressure ratio, duct length, expansion ratio, and length-to-diameter ratio significantly impact base pressure and reattachment length [3-6]. Passive control methods like ribs and cavities are generally explored for improving base pressure and reducing drag in suddenly expanded flows. Khan *et al.,* [1] conducted numerical and experimental investigations of various shapes of the ribs in suddenly expanded flows. They compared numerical results with experimental results and applied machine learning models. Their findings show that the rib shapes influence flow stability [7-19]. Sajali *et al.,* [20] conducted a numerical analysis of flow fields across a non-circular cylinder.

Khan *et al.,* [21] studied dimples as a passive control method in subsonic flows. Their study showed that dimples effectively change base pressure. Fiqri *et al.,* [22] and Aqilah *et al.,* [23] investigated the cavity as a control method in suddenly expanded flows. Their study demonstrated improved pressure regulation. Active control techniques, such as micro-jets or control jets in supersonic flows, have been discovered for base pressure regulation in suddenly expanded flows. Their findings show that the control jets effectively control base pressure [24-26]. Computational Fluid Dynamics (CFD) studies high-speed flows, surface pressure distribution, heat transfer, and aerodynamic stability. Shaikh *et al.,* [27] and Shamitha *et al.,* [28] have studied analytical and CFD-based research on pressure distribution on the nose of a 2D wedge in high-speed flows. Their finding shows that the results obtained by CFD analysis significantly agreed with the analytical and experimental results [27-41].

Based on the above literature, extensive research on suddenly expanded flows using passive and active control techniques has been carried out. However, gaps continue in the existing literature, and most studies have focused on sonic and supersonic Mach numbers. However, research on flow control at lower Mach numbers (subsonic to transonic) remains insufficient. Also, it needs to be done

to optimize the rib shape and its location as passive control techniques. The rib, in the D shape with different orientations, has not been studied in the literature, nor has the D-shaped rib and rib placement at various locations been extensively covered.

3. Finite Volume Method

3.1 Governing Equations

The following hypotheses are taken into consideration:

i. Turbulent flow is considered because of the turbulent viscous dissipation effects.
ii. The fluid's viscosity varies with temperature and is compressible.
iii. At atmospheric pressure, the flow exits the duct.
iv. While scanning the literature, we found that the internal flow k-epsilon turbulence model is the best, as it gives reasonably good results. Sutherland's three-coefficient viscosity model is expressed as follows:

$$\mu' = \mu'_o \left(\frac{T_a}{T_{a,o}}\right)^{3/2} \frac{T_{a,o}+S\prime}{T_a+S\prime} \tag{1}$$

The reference viscosity value in kg/m-s is denoted as μ'_o, where μ' represents the viscosity. T_a denotes static temperature; K represents the temperature of a standard reference, and S' is the temperature-dependent Sutherland constant. Three-dimensional continuity equation for compressible flow: The equation for mass balance is as follows:

$$\frac{\partial \rho}{\partial t} + \underline{\nabla} \cdot (\rho \underline{V}) = 0 \tag{2}$$

where the fluid's velocity is denoted by V. The equation for momentum balance is:

$$\frac{\partial}{\partial t}(\rho \underline{V}) + \underline{\nabla} \cdot (\rho \underline{V}\underline{V}) + \underline{\nabla} p = \underline{\nabla} \cdot \left[2\mu \left(\underline{\nabla V}\right)_o^s\right] + \underline{\nabla} \cdot (\tau_{=Re}) \tag{3}$$

where $\left(\underline{\nabla V}\right)_o^s = \left(\underline{\nabla V}\right)^s - \frac{1}{3}(\underline{\nabla} \cdot \underline{V})\underline{I}$, $\left(\underline{\nabla V}\right)^s = \frac{\underline{\nabla V} + \underline{\nabla V}^T}{2}$ and $\tau_{=Re}$ is the turbulent stress tensor. The formulae for total energy are as follows:

$$\frac{\partial}{\partial t}\left[\rho\left(\frac{1}{2}V^2 + u_{int}\right)\right] + \underline{\nabla}\left[\rho\left(\frac{1}{2}V^2 + u_{int}\right)\underline{V}\right] = \underline{\nabla}\left(\lambda \underline{\nabla} T - p\underline{V} + 2\mu \underline{V} \cdot \left(\underline{\nabla V}\right)_o^s + \underline{V} \cdot \tau_{=Re}\right) \tag{4}$$

where u_{int} is the internal energy, and λ is the thermal conductivity. Many internal flow simulations use the k-epsilon turbulence model due to its affordability, resilience, and sufficient accuracy. The Ansys Fluent program incorporates the k-epsilon (ε) turbulence model used in this research. The K-equation allowed us to calculate the turbulent kinetic energy.

$$\frac{\partial}{\partial t}(\rho k) + \underline{\nabla} \cdot (\rho \underline{V} k) = \underline{\nabla} \cdot \left[(\mu + \frac{\mu_t}{\sigma_k})(\underline{\nabla} k)\right] - \rho\varepsilon + M_x \tag{5}$$

The turbulent kinetic energy dissipation rate is denoted by ε, the turbulent Prandtl number is σ-k, and the word Mx is the turbulence generation. Precisely, the dissipation (or (-equation)) is controlled by:

$$\frac{\partial(\rho\varepsilon)}{\partial t} = -\underline{\nabla}\cdot\left(\rho\varepsilon\vec{V}\right) + \underline{\nabla}\cdot\left[\left(\mu + \frac{\mu_T}{\sigma_\varepsilon}\right)\nabla\varepsilon\right] - C_1 f_1\left(\frac{\varepsilon}{k}\right)M - C_2 f_2\frac{\varepsilon^2}{k} \quad (6)$$

where $\mu_t = \rho f_\mu C_\mu k^2/\varepsilon$ denotes turbulent viscosity, and the arbitrary constants are denoted as $\overline{C_\mu} = 0.09$, $\overline{C_1} = 1.44$, $\overline{C_2} = 1.92$, $\overline{f_\mu} = 1$, $\sigma_k = 1.0$ and $\sigma_\varepsilon = 1.3$.

3.2 Geometry and Modelling

The finite volume technique (FVM) was employed to delve further into this investigation. The CFD simulation used the ANSYS FLUENT software to assess the nozzle's fluid flows. We are examining the impact of the rib's D-shaped geometry using a passive control method. The orientations of the quarter rib are shown in Figures 2 (a) and 2(b).

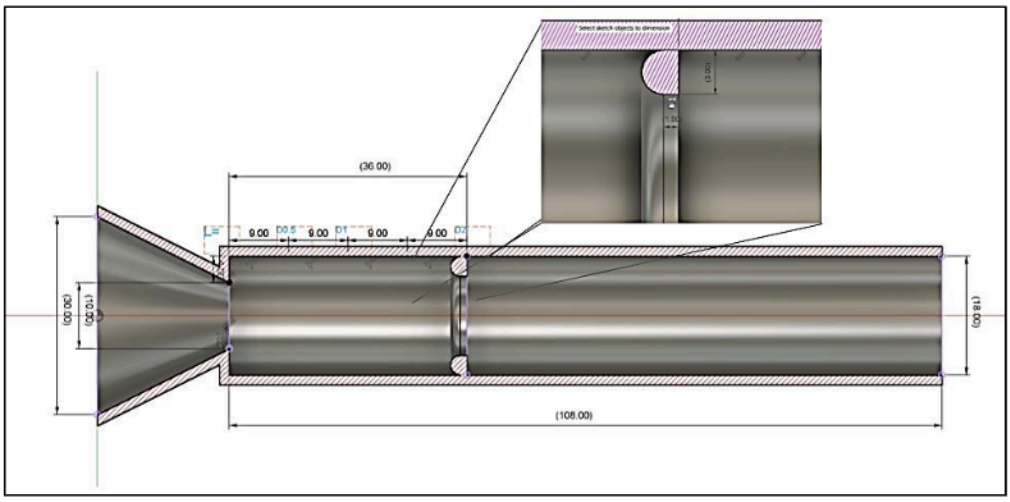

(a)

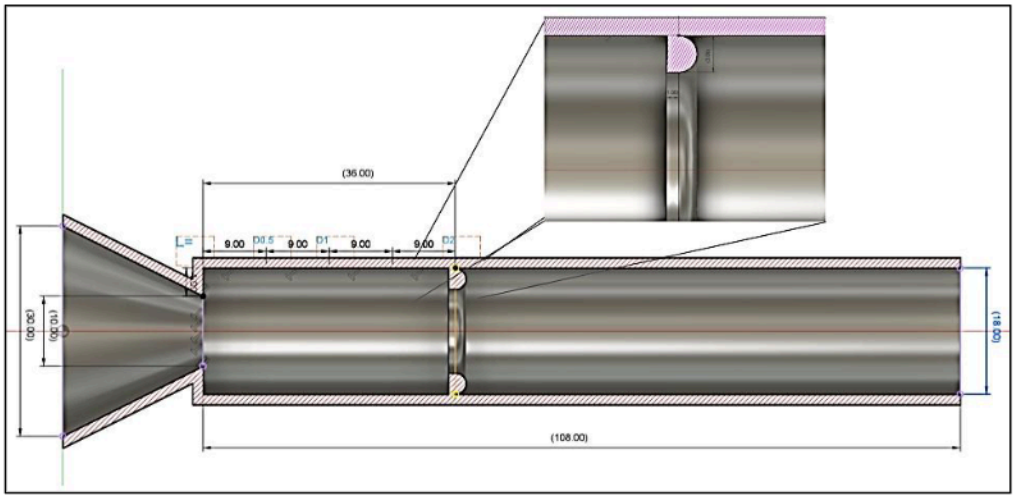

(b)

Fig. 2. Orientation one of the rib (a) Orientation 1 (b) Orientation 2

3.3 Meshing and Boundary Conditions

A crucial part of the CFD process is meshing. In this case, the 2D model is of the structured mesh type by choosing the free-face mesh type. When the constructed structured mesh type was used,

elements were given sizes according to each line (edge) length. The lines were utilized to apply the element size, and elements with identical forms were created using face meshing. The mesh independence check is done. Figures 3(a) to 3(c) below shows the mesh's element type and size tested during the mesh independence check for geometry without rib and with rib at both orientations.

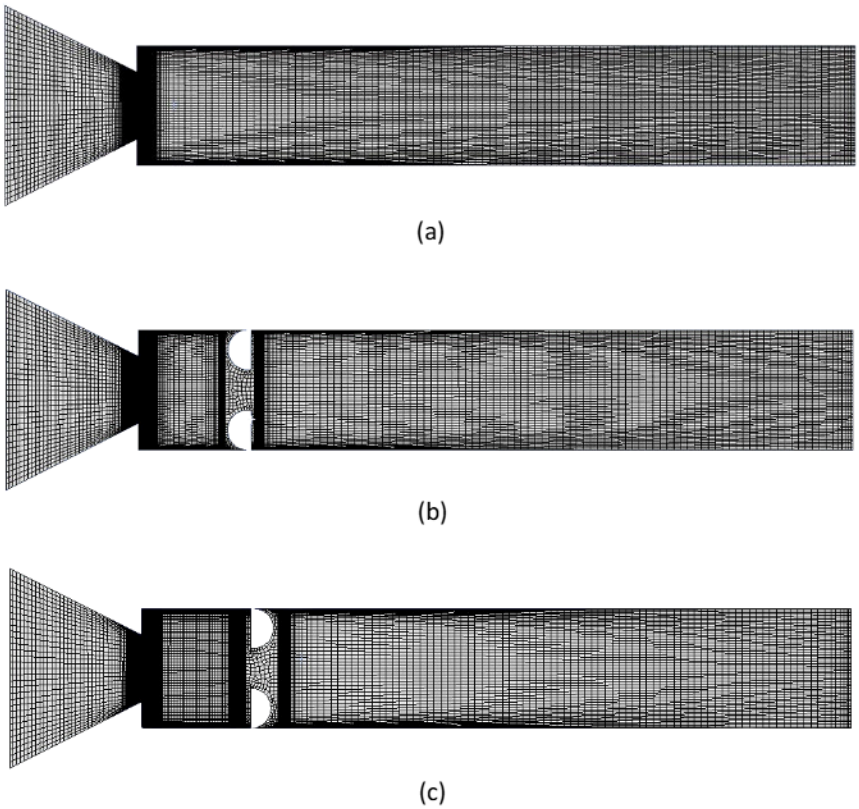

Fig. 3. Mesh model (a) Without rib (b) Rib with orientation 1 (c) Rib with orientation 2

3.4 Assumptions and Fluid Properties

Assumptions are used to replicate the flow activities in the precise physical environment. Appropriate mathematical and numerical models are selected to make the governing equations. To solve the governing equations simultaneously, numerical modeling requires choosing the appropriate mathematical models, such as the governing equations, boundary conditions, mesh quality, and numerical method. Despite its limitations in accurately representing physical phenomena, the computational method has been trusted for decades and offers sufficient insight into flow behavior. As a result, this calls for careful consideration of elements that closely resemble the flow behavior. This study pinpoints the presumptions that jeopardize the precise physical state. The following are the assumptions and characteristics covered in this study:

i. The flow is assumed to be a steady 2D flow because geometry is symmetric. Hence, the assumption that the flow is 2-D is justified.
ii. The density of the air is variable as the flow is compressible. The inlet pressure is the gauge pressure at that Mach number and NPR, and at the outlet of the duct, the gauge pressure at the outlet is zero.

iii. Turbulent flow significantly impacts turbulent viscous dissipation at a given flow velocity, so it is considered.
iv. The viscosity of the fluid is dependent on temperature.
v. At standard atmospheric pressure, the flows leave the duct. At normal ambient pressure, they do not.

Since the flow via the nozzle is considered turbulent, the compressible flow field is represented by the k-epsilon standard model. The subsequent equations most appropriately characterize the turbulent flow.

3.5 Geometry of the Model

The ANSYS Workbench program utilized fluid flow (Fluent) analytical techniques throughout the computational fluid dynamics (CFD) procedure. The model was generated via a Design Modeler. Figure 4 depicts a converging nozzle that abruptly widens into a duct with five ribs. Rathakrishnan [42] experimental setup, the dimensions of the convergent-divergent nozzle with a suddenly expanded duct are as listed in Table 1.

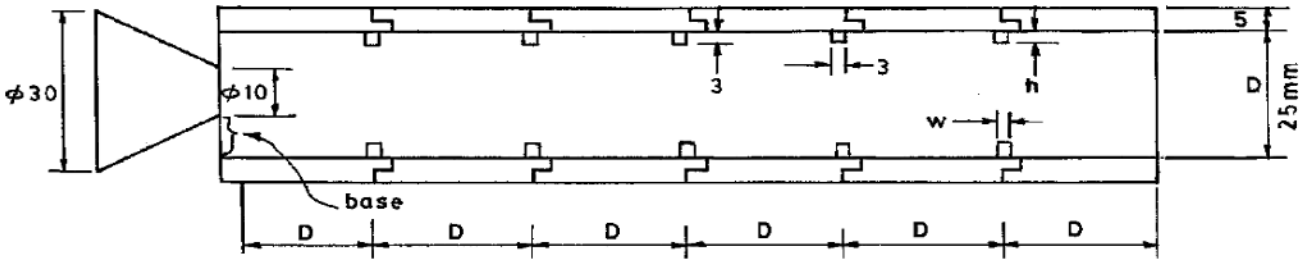

Fig. 4. Duct with five ribs used in an experimental study [42]

Table 1
The geometries of the validation model

Parameters	Dimensions
Nozzle inlet diameter	30 mm
Nozzle outlet diameter	10 mm
Duct diameter (D)	25 mm
Duct length (L)	Varies from 1D to 6D
Converging length	20 mm
Rib width	3 mm
Rib height	Varies from 1 mm to 3 mm

3.6 Validation of Previous Work

According to Rathakrishnan [42], the prior work was performed at aspect ratios of 3:3, 3:2, and 3:1; an area ratio of 6.25; L/D ranging from 1 to 6; pressure ratios of 1.141, 1.295, 1.550, 1.707 and 2.458; and nozzle exit Mach numbers of 0.44, 0.62, 0.82, 0.91 and 1.0. However, in a prior publication by Rathakrishnan [42], the result from Figure 4 with NPR (P01/Pa) 2.458 and models with control in the form of ribs with aspect ratios 3:2 and 3:3 was chosen to be compared to the current work. The simulation is supported by Rathakrishnan [42] experimental work, which used five ribs positioned at equidistant intervals in the duct, as illustrated in Figure 4. The results of base pressure fluctuation with NPR of 2.458 and L/D ranging from 2 to 6 are obtained. The study is repeated to validate the numerical results of a model with control over different rib aspect ratios [42].

Figure 5 demonstrates the current and earlier studies' base pressure ratio data curves [42]. The experimental values were denoted by dotted lines, while the simulation results obtained using ANSYS Fluent were represented by straight lines. The present numerical analysis exhibited a percentage discrepancy of less than 10% compared to the previous experimental study. Consequently, the current work met the criteria for acceptability. The curves exhibited a consistent pattern, with each point close to the subsequent one. As a result, based on the table and graph described before, the validation of the current work was successful.

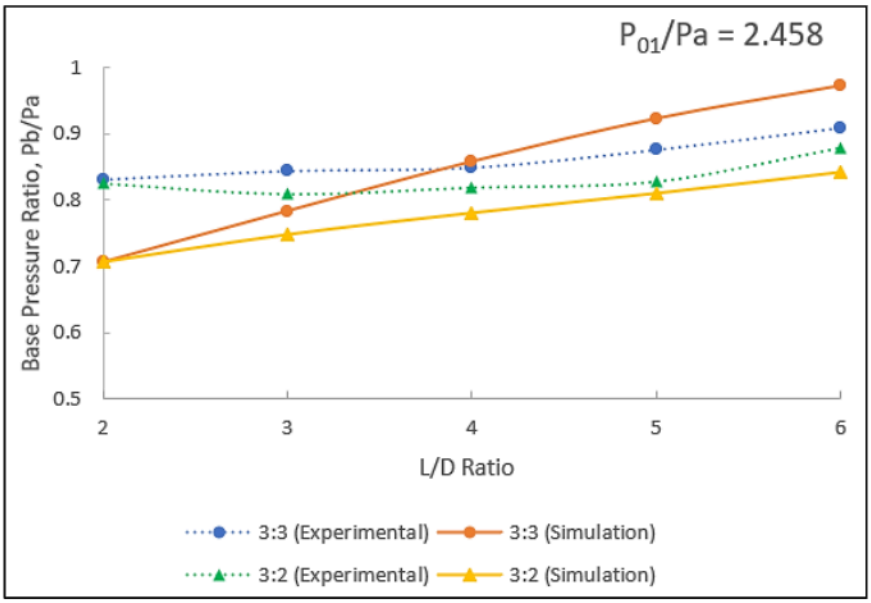

Fig. 5. Validation of previous work by Rathakrishnan [42]

3.7 Mesh Independence Study

Table 2 provides data from a mesh independence study, a crucial step in computational simulations to ensure that the results remain consistent regardless of the mesh refinement level. The element sizes range from the course to the finest, with corresponding node and element counts for each mesh configuration. As the mesh becomes finer, the number of nodes and elements increases significantly, from 1,284 nodes and 1,145 elements in the coarsest mesh to 1,354,262 nodes and 1,351,303 elements in the finest mesh. This study aims to determine the optimal mesh size for accurate simulations without unnecessary computational expense. The table shows a notable increase in nodes and elements as the mesh is refined. The coarsest mesh has relatively few nodes and elements, which means lower computational cost but potentially less accuracy. Conversely, the finest mesh offers the highest resolution at the expense of significant computational resources. The medium and fine meshes provide intermediate levels of refinement, offering a balance between accuracy and efficiency.

Table 2
Mesh independence study

Element size	Coarsest	Coarse	Medium 1	Medium 2	Fine	Finer	Finest
Nodes	1875	2632	9468	18918	140327	412132	2133890
Elements	1726	2451	9177	18525	139315	410410	2129987

Based on the trends in node and element numbers, the finest mesh will likely produce the most accurate results (Figure 6). However, continuing to refine the mesh beyond a certain point may offer diminishing returns in terms of accuracy while significantly increasing computational time. A critical assessment of this table would suggest that the "fine" or "finer" mesh configurations may represent the best balance between accuracy and computational efficiency. These configurations substantially increase nodes and elements compared to the medium meshes without reaching the computational expense of the finest mesh. If simulation results do not significantly change between the fine and finest meshes, further refinement to the finest mesh is unnecessary, as it would only increase the computational time without added benefit. Thus, the fine or finer mesh sizes are likely the best choices for further simulation.

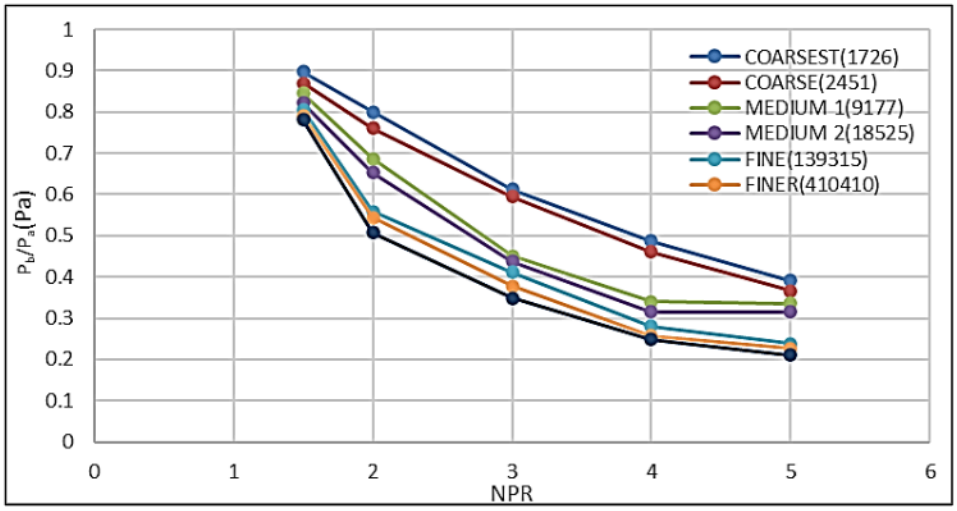

Fig. 6. Grid independence test

4. Results and Discussions

This research assesses the effect of D-shaped ribs on the larger duct's base flow and development. When the rib's straight portion faces the base region, orientation one is given a nomenclature. The other side of the ribs is named orientation 2 when the base recirculation region faces the curved surface. Numerical simulations were conducted for both orientations. While performing the simulations, the ribs were oriented in two directions. The first was when the straight side of the rib was towards the base region, and the second was when the curved part faced the base recirculation zone. In addition, the larger duct diameter of 18 mm and the noticeably high area ratio of 3.24 should be mentioned while analyzing the data. When the flow exits the nozzle, it will expand freely and reattach with the enlarged duct to a place different from the ideal one for an intense vortex at the base because of the additional relief provided to the flow. Because of this procedure, the impact of NPR on base pressure becomes negligible in large areas.

Before delving into the base pressure findings resulting from the ribs, it would be more beneficial to comprehend the flow mechanics involved in the shear layer exhaustion process in a larger duct. When the Mach number M < 1, the boundary layer will get divided and reattach itself to the duct when it exits the tip. The divided region will have one or more vortices since the initial vortex will be close to the base and reasonably strong. We designate the center vortex as this vortex. This device, which functions as a pump, will move fluids from the base region to the primary jet on the shear layer's edge. Because of this forcing action, low pressure will exist in the recirculation. Pushing action, however, is too irregular given that this vortex spread is recognized as cyclical. This irregular pattern

results in discrepancies in the base pressure. It is discovered that these changes in base pressure are negligible.

We consider mean base pressure values in our data analysis. The vortex cyclicity may cause the entire flow pattern in the enlarged image to fluctuate. Under specific geometrical and inertia conditions, these oscillations can become extremely severe. The area ratio, Mach number, reattachment length, and degree of expansion are the primary factors that affect the strength of the core vortex at the base, which fluctuates. Figure 2(a) shows the orientation 1 of the D-shaped rib where the separated flow interacts with the flat surface of the rib. In this section, we will discuss the influence of the rib on manipulating the base pressure for this orientation, and numerous rib locations for various duct sizes will be debated.

4.1 Base Pressure Results for Rib Orientation 1

4.1.1 Base pressure results for rib location 0.5D

Figures 7 (a) to (f) show the base pressure results when the rib is located at 0.5D for NPRs ranging from 1.5 to 5 for duct sizes from 1 to 6. Figure 7(a) shows that ribs with radii 2 and 3 mm have base pressure ratios of 3 and 4.7, whereas a 1 mm rib radius results in base pressure ratios of less than one. A 1 mm rib radius is effective from NPR = 3 and above. Such high values of the base pressure are attributable to the fact that the duct diameter is small, and the reattachment length is expected to be around L/D = 1 to 1.5. Under these conditions, when passive control is employed, the flow is blocked, which increases the base pressure. Also, it should be remembered that when the rib is located at L/D = 1 and above, it will give a better picture of the flow development in the duct and base pressure gain. The rib location at 0.5D may not provide clarity, as the flow is in the transition stage.

Similar results are seen for other duct sizes as the rib location is fixed, and the variations in the duct lengths have a marginal influence on the flow inside the duct. There are slight changes in the base pressure values due to the impact of the ambient atmospheric pressure. Besides this, we have not observed any significant changes in the flow field. For rib radius 2 and 3 mm, the base pressure increases from NPR = 1.5 and above. The 1 mm radius is the smallest one, and its impact is seen when the nozzles are under-expanded, and the minimum under-expansion needed is P_e/P_a = 1.5. Control becomes effective again when nozzles flow under a favorable pressure gradient.

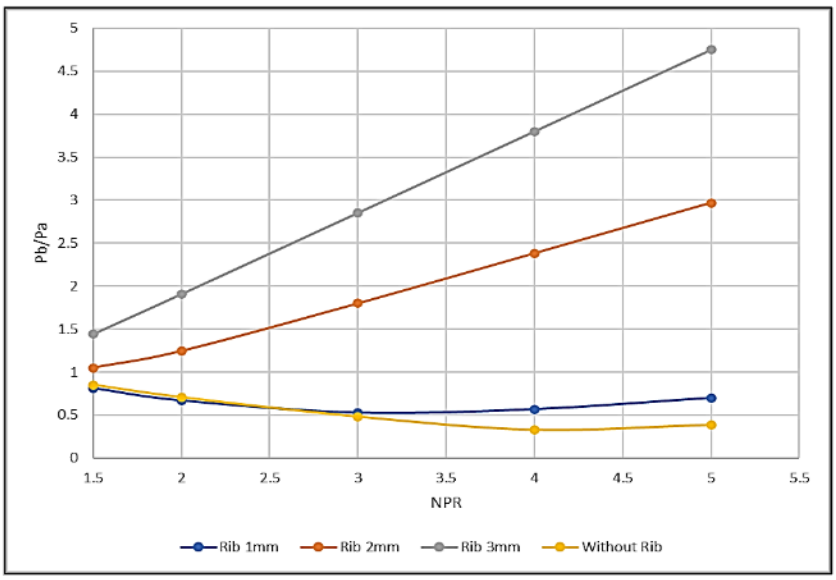

(a)

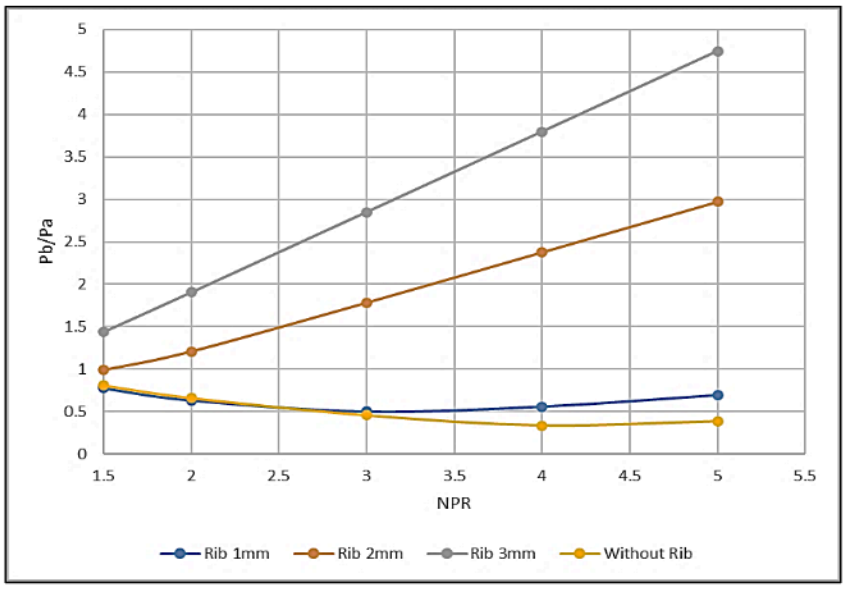
Pb/Pa
NPR
Rib 1mm
Rib 2mm
Rib 3mm
Without Rib

(b)

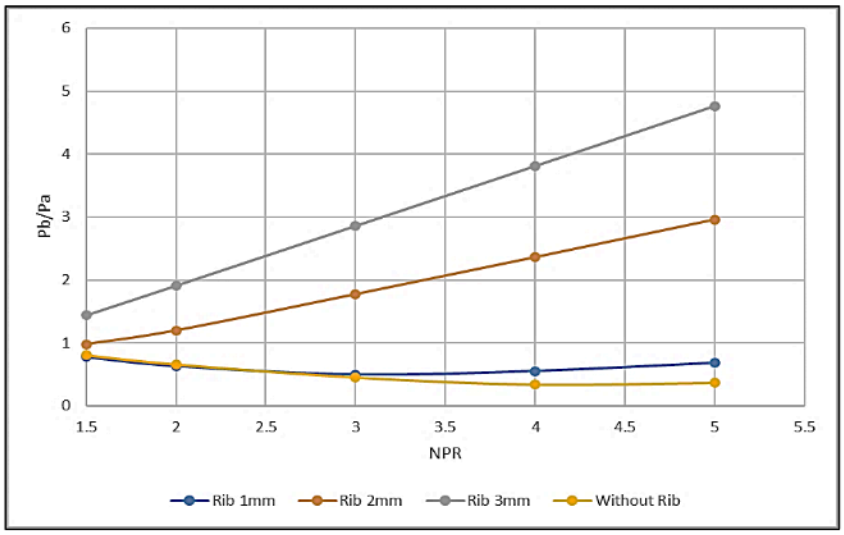
Pb/Pa
NPR
Rib 1mm
Rib 2mm
Rib 3mm
Without Rib

(c)

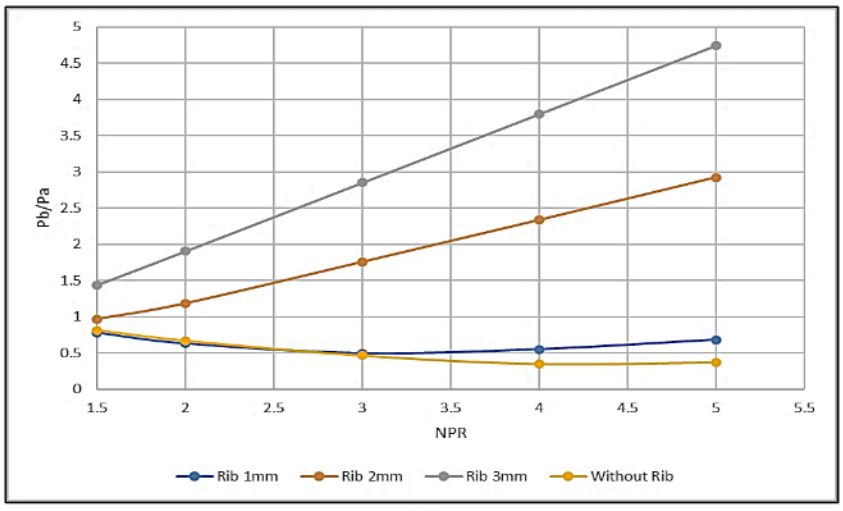
Pb/Pa
NPR
Rib 1mm
Rib 2mm
Rib 3mm
Without Rib

(d)

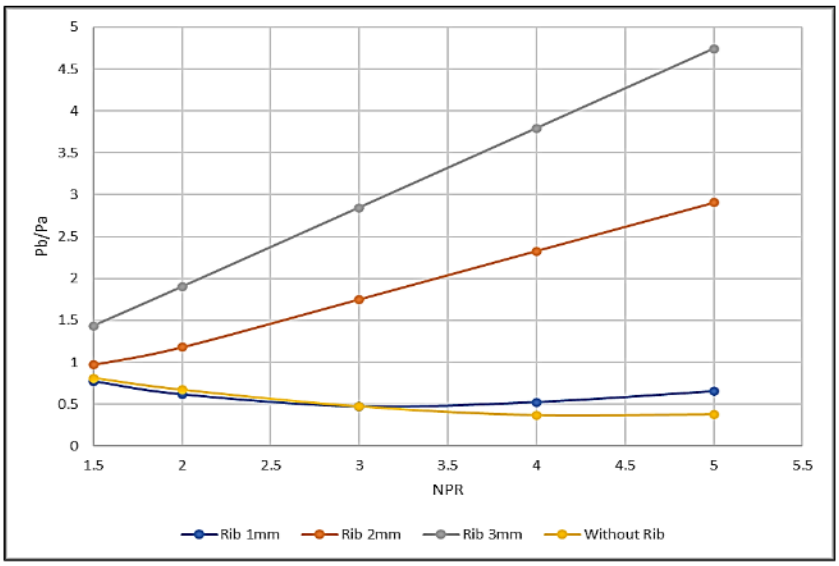

(e)

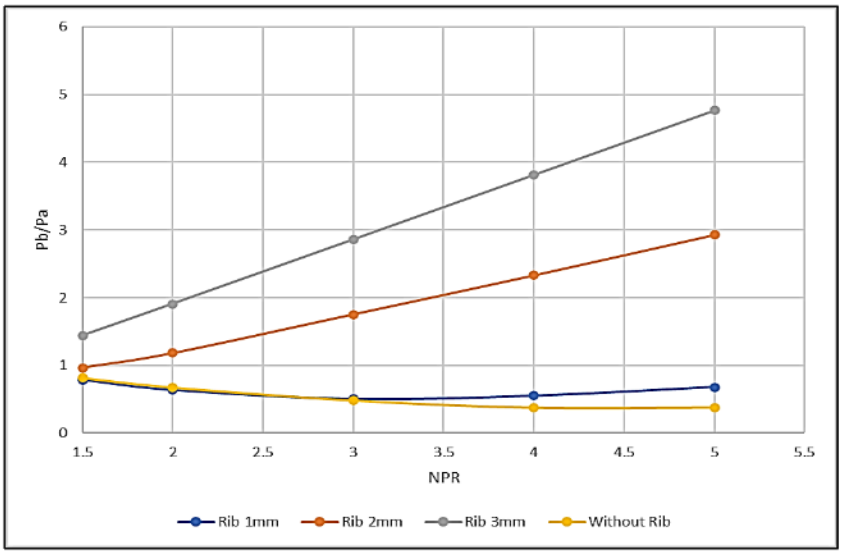

(f)

Fig. 7. Base pressure variation with NPR at rib location at 0.5D for various duct sizes and rib orientation 1 (a) L/D = 1 (b) L/D = 2 (c) L/D = 3 (d) L/D = 4 (e) L/D 5 (f) L/D 6

4.1.2 Base pressure results for rib location 1D

When the rib is located at a 1D location, the outcomes of this study are shown in Figures 8(a) to 8(e) at various levels of expansion and duct lengths. Figure 8(a) displays the results for L/D = 2. When we compare the results for this rib location and the previous location where the rib is located at L/D = 0.5, due to the shift in the rib location, there is a change in the base pressure results for a rib radius of 2 mm, the base pressure ratio has increased from 3 to 3.4, and for remaining rib radius of 1 mm and 3 mm, there is no change in the base pressure. This pattern in the base pressure is related to the secondary vortices created due to the presence of a passive control mechanism; in the case of the 3 mm rib, it has attained the maximum value of the base pressure, and any change in the location of the rib does not result in any change in the base pressure.

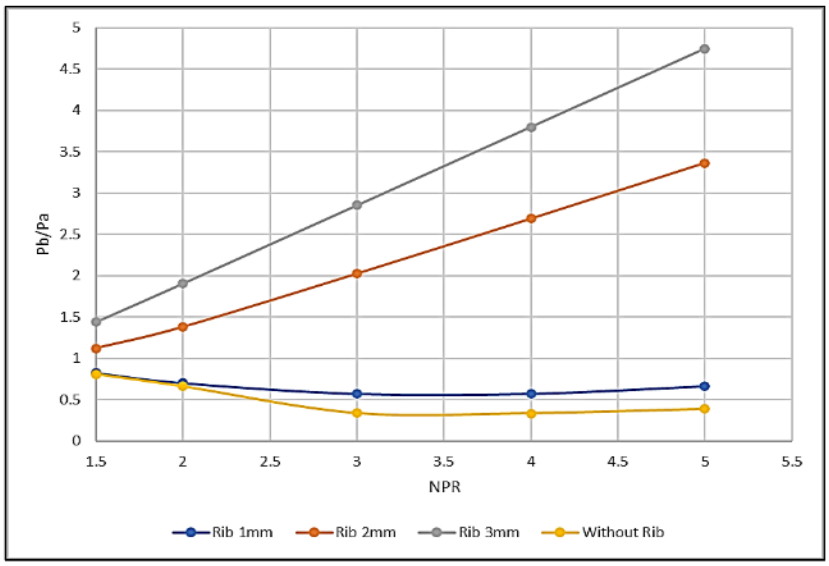
Pb/Pa
NPR
Rib 1mm
Rib 2mm
Rib 3mm
Without Rib

(a)

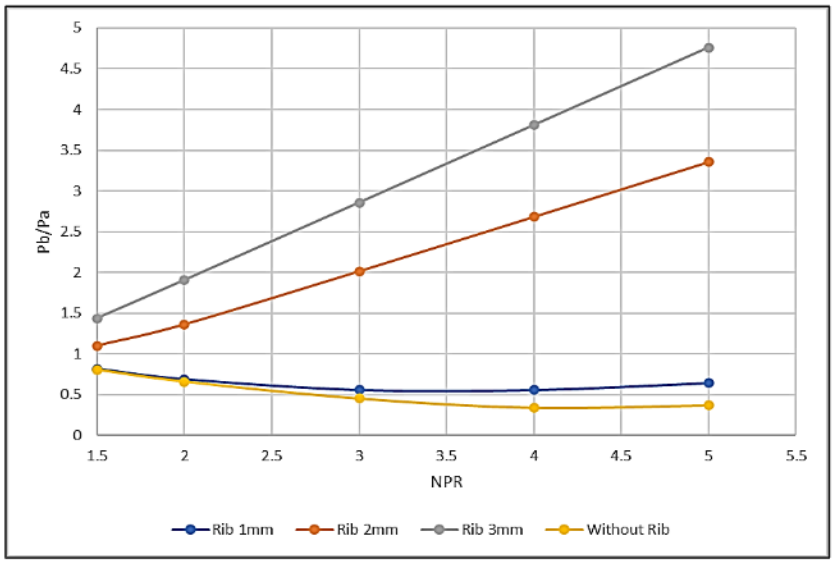
Pb/Pa
NPR
Rib 1mm
Rib 2mm
Rib 3mm
Without Rib

(b)

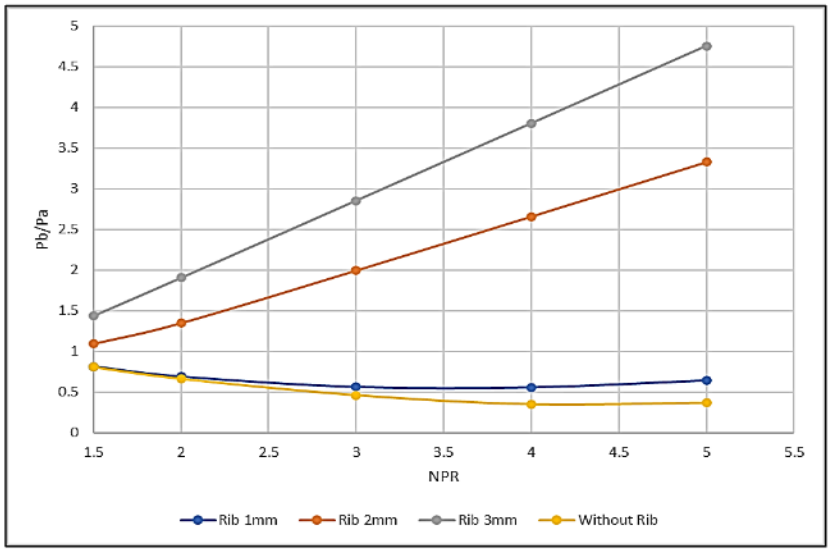
Pb/Pa
NPR
Rib 1mm
Rib 2mm
Rib 3mm
Without Rib

(c)

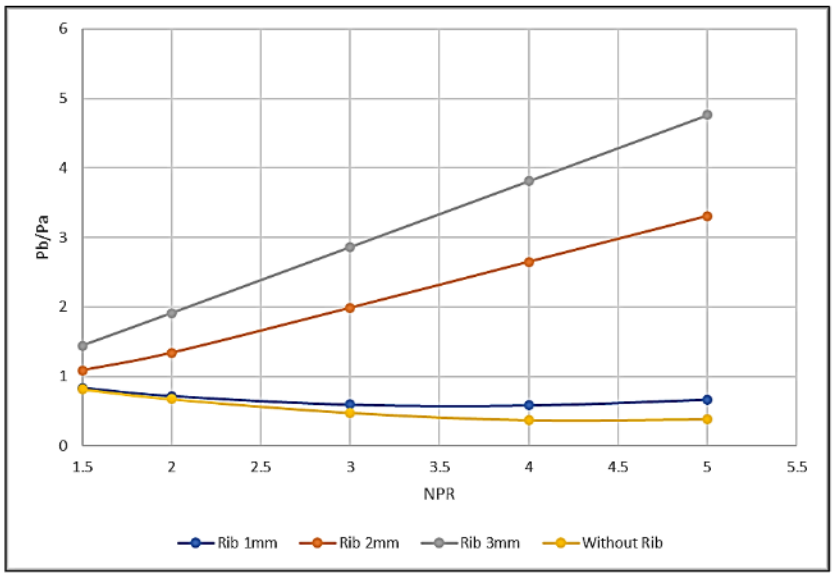

(d)

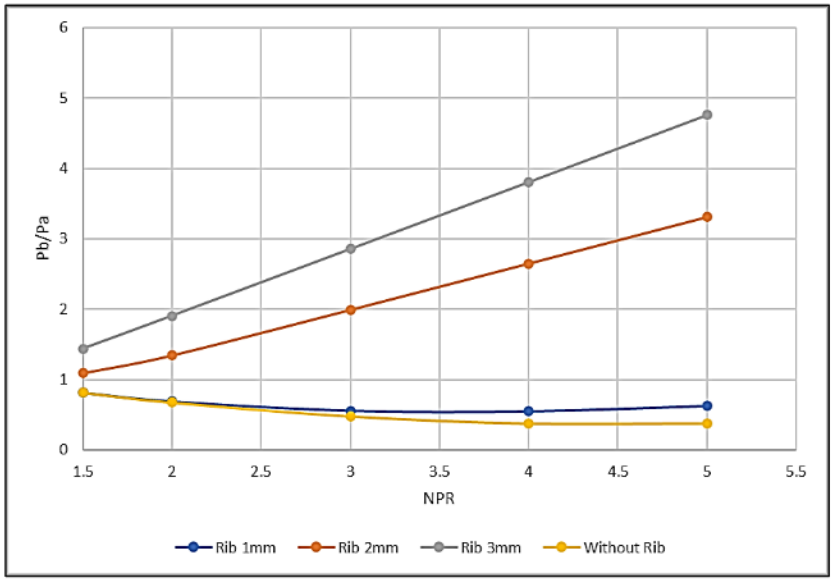

(e)

Fig. 8. Base pressure variation with NPR at rib location at 1D for various duct sizes and rib orientation 1 (a) L/D = 2 (b) L/D = 3 (c) L/D = 4 (d) L/D = 5 (e) = L/D 6

For the lowest rib radius, the secondary vortex is weak and unable to impact the flow field. Similar results of base pressure are seen for duct length-to-diameter ratios of 3, 4, 5, and 6, as shown in Figures 8(b) to (e). There are minor changes in the base pressure values due to increased duct size and the influence of the back pressure.

4.1.3 Base pressure results for rib located at 1.5D

Base pressure results for rib located at 1.5D are shown in Figures 9(a) to 9(e) for NPRs in the range from 1.5 to 5 and duct length-to-diameter ratios of 2, 3, 4, 5, and 6. Figure 9(a) shows that the base pressure values are almost identical to those in the previous case, where the rib was located at 1D. It is well known that the base pressure in the separated base region will depend on the following parameters: duct diameter, expansion level, reattachment length, etc. For this duct diameter, the

reattachment length seems to be at 1D. If we place any control mechanism beyond the reattachment length, the flow control mechanism will not yield beneficial results. Therefore, it may be concluded that the optimum location of the rib is 1D. As discussed above, any variation in the rib locations will not yield any benefits, and the same pattern is seen for other duct lengths. There is not much difference in the base pressure, except minor changes are seen due to the impact of the ambient atmospheric pressure.

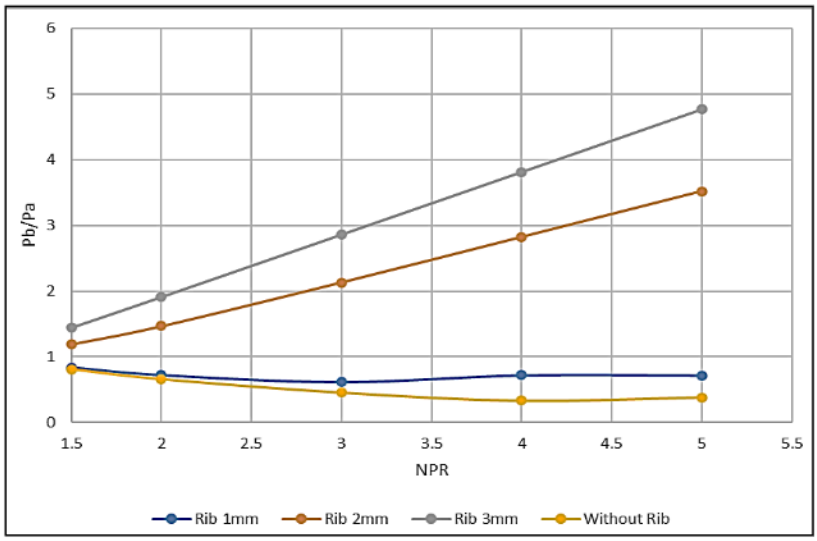

(a)

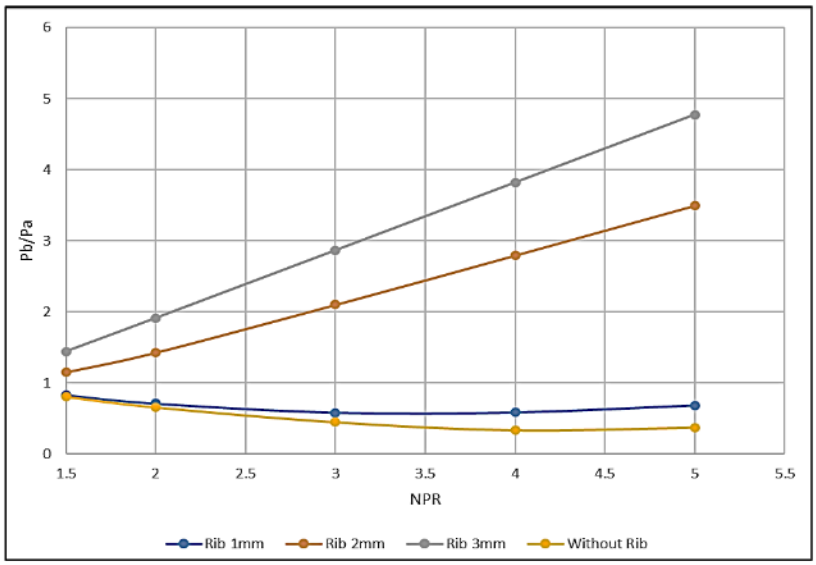

(b)

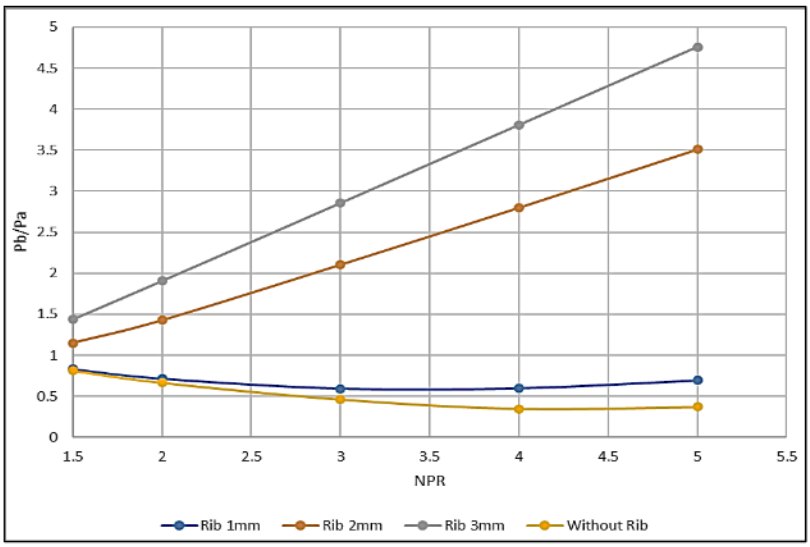

(c)

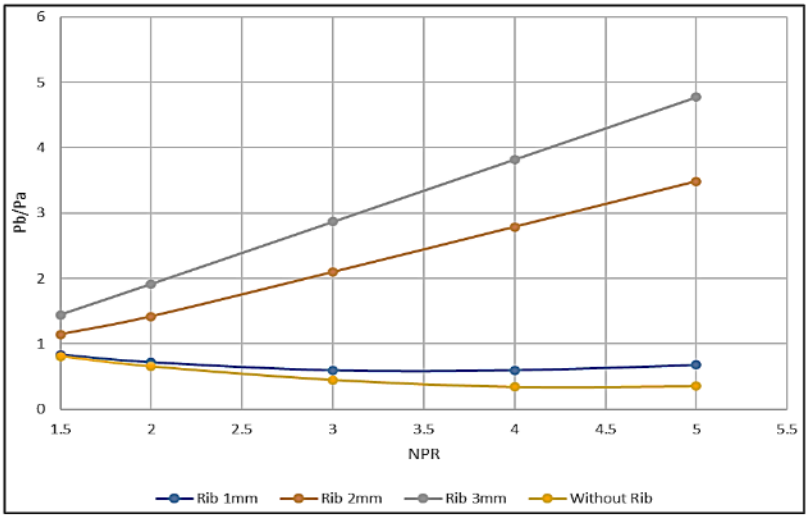

(d)

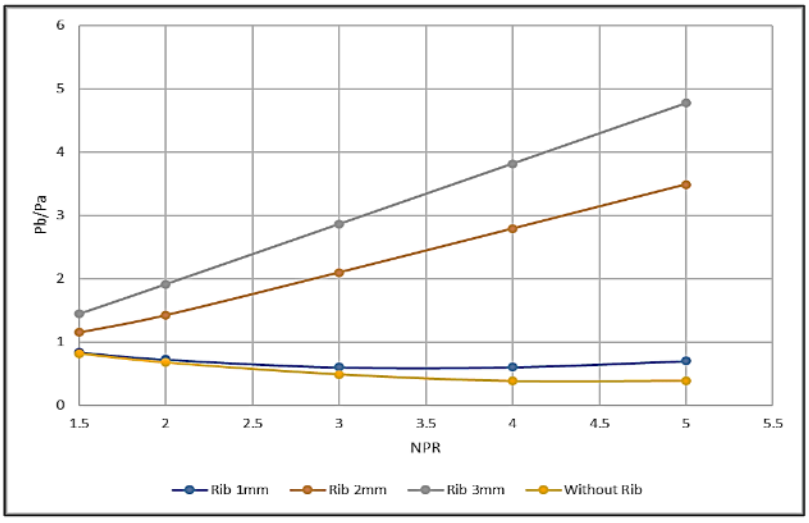

(e)

Fig. 9. Base pressure variation with NPR at rib location at 1.5D for various duct sizes and rib orientation 1 (a) L/D = 2 (b) L/D = 3 (c) L/D = 4 (d) L/D = 5 (e) L/D = 6

4.1.4 Base pressure results for rib located at 2D

For the Rib location at 2D, the findings of this study are shown in Figures 10 (a) to 10(d) as a function of the nozzle pressure ratio for a given duct length. As discussed earlier, there is no change in the values as the maximum gain in the base pressure has been achieved, and the base pressure has become independent of the rib location and duct lengths.

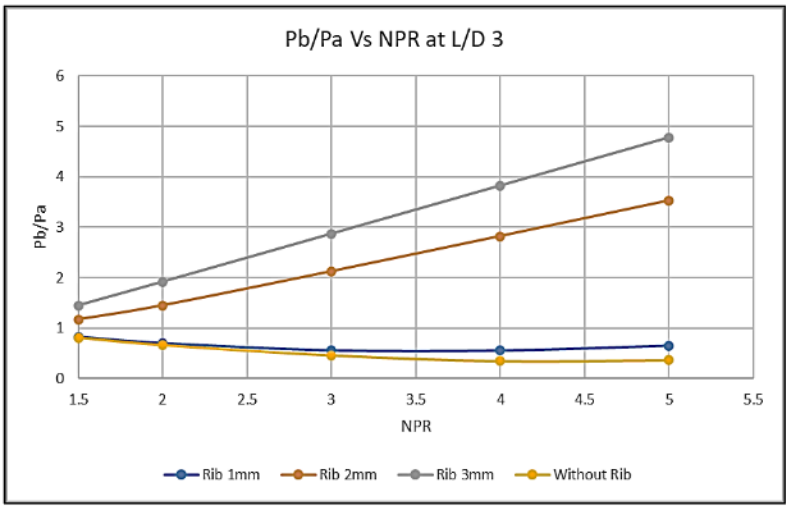

(a)

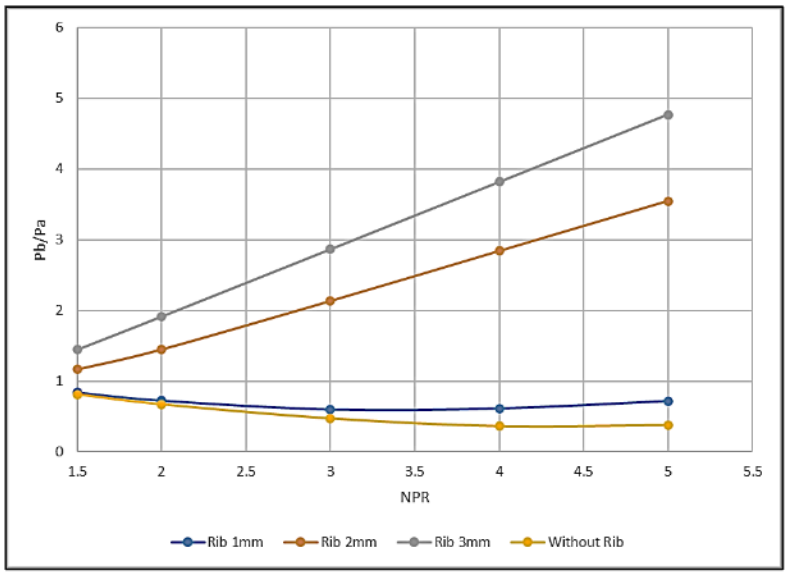

(b)

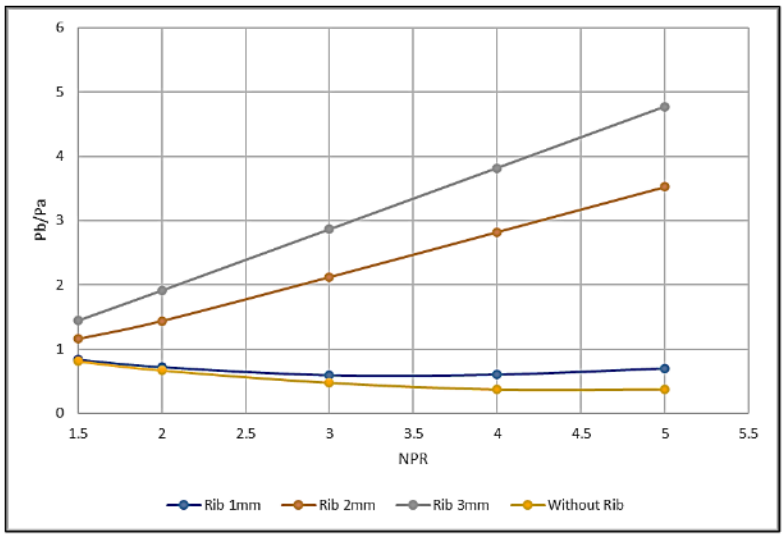

(c)

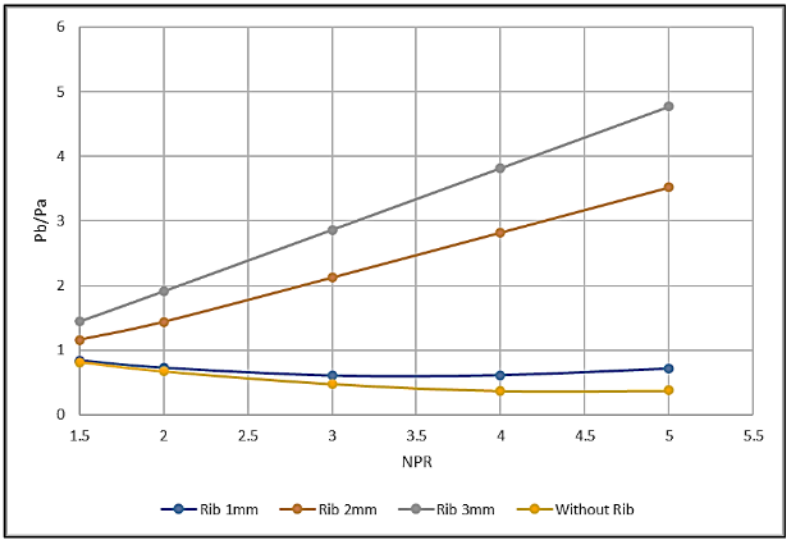

(d)

Fig. 10. Base pressure variation with NPR at rib location 2D for various duct sizes and rib orientation 1 (a) L/D = 3 (b) L/D = 4 (c) L/D = 5 (d) L/D = 6

4.1.5 Base pressure results for rib located at 3D

When the rib is located at 3D, the outcomes of this study are displayed in Figures 11(a) to 11(c), where Base pressure ratio Vs. Nozzle Pressure Ratio is plotted for various ribs and duct lengths and radii. The results found no variations in the base pressure values despite changes in the location of the rib—the physics behind this trend we have already discussed.

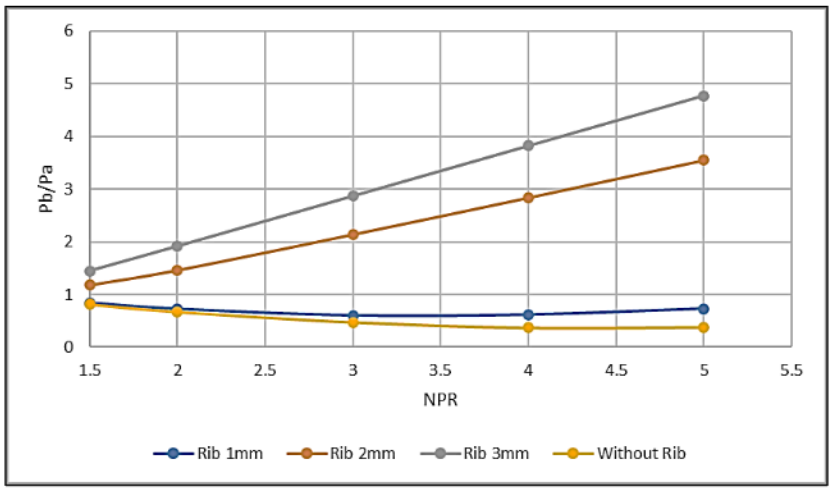

(a)

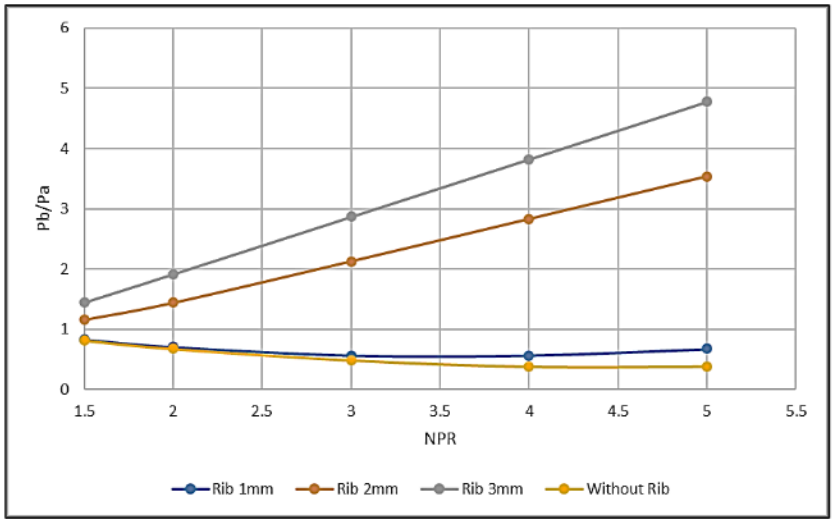

(b)

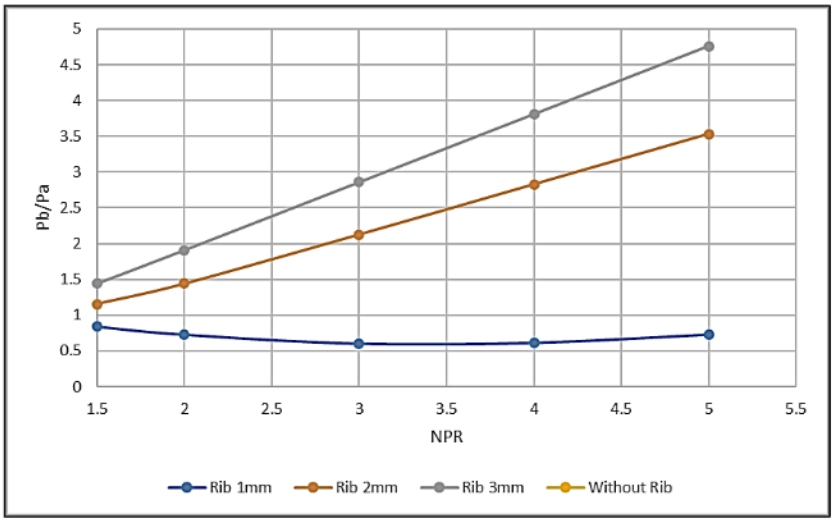

(c)

Fig. 11. Base pressure variation with NPR at rib location at 3D for various duct sizes and rib orientation 1 (a) L/D = 4 (b) L/D = 5 (c) L/D = 6

4.2 Base Pressure Results for Rib Orientation 2

Figure 2(b) shows orientation 2 of the rib where the shear layer faces the flat part of the rib, and it is expected that for this orientation of the rib, there will be an increase in the base pressure as compared to orientation one, where the curved part of the rib is facing the shear layer.

4.2.1 Base pressure results for rib located at 0.5D

Figures 12(a) to 12(f) show the outcomes of this study for orientation two, where the flat portion of the rib sees the flow from the nozzle for the rib location as 0.5D as a function of nozzle pressure ratio for various duct sizes. Figure 12(a) shows that, as far as base pressure for rib radius 3 mm is concerned, it is identical to orientation one. However, when we look at the base pressure resulting from the rib radius of 1 mm and 2 mm, we see a considerable increase in the base pressure values. In the case of a 1 mm rib radius, till the flow is choked, there is a marginal decrease in the base pressure. Later, once the flow has become under-expanded, there is a progressive increase in the base pressure, and at around NPR = 4, the base pressure is almost equal to the atmospheric pressure. However, when we look at the base pressure values for a rib radius of 2 mm, the base pressure value equals the ambient atmospheric pressure. With a further increase in the base pressure, the base pressure ratio becomes three.

When we look at the base pressure resulting from the other duct lengths, it is found that the base pressure values are nearly the same, with slight variations in the values. These variations are attributed to the change in the duct lengths and the impact of the atmospheric pressure.

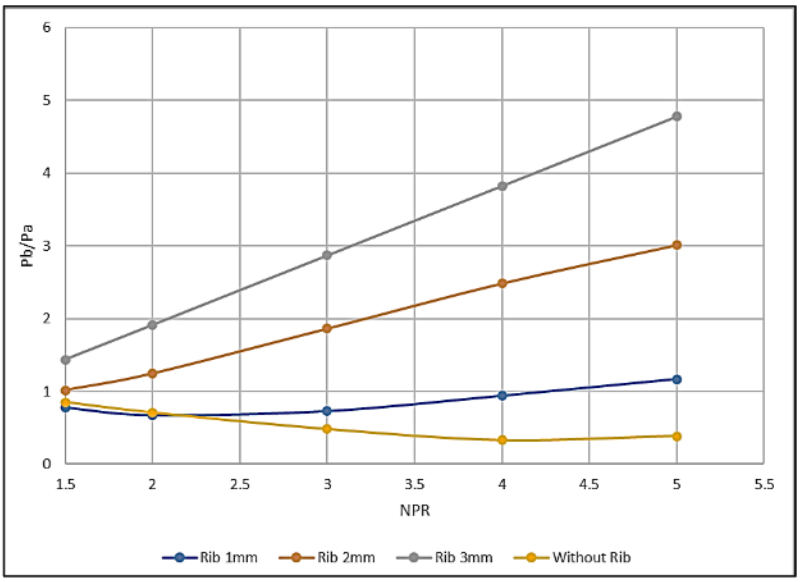

(a)

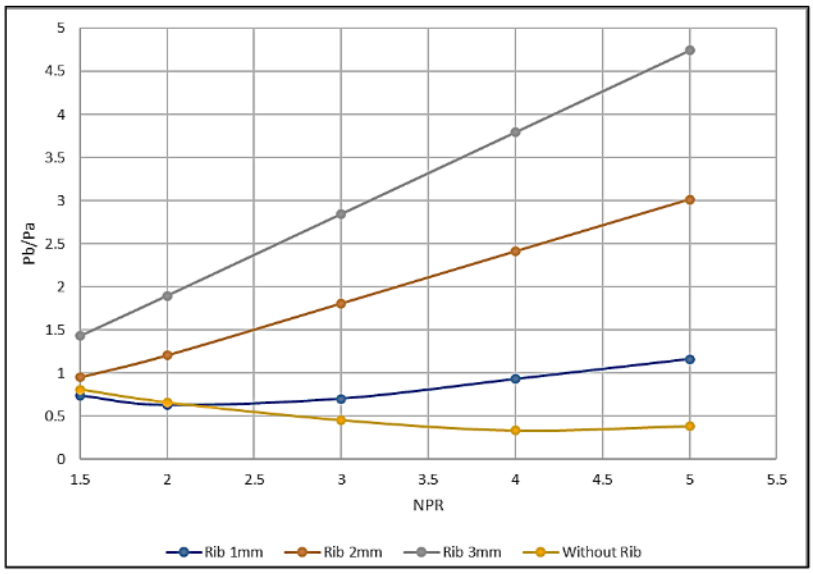
Pb/Pa
NPR
Rib 1mm
Rib 2mm
Rib 3mm
Without Rib

(b)

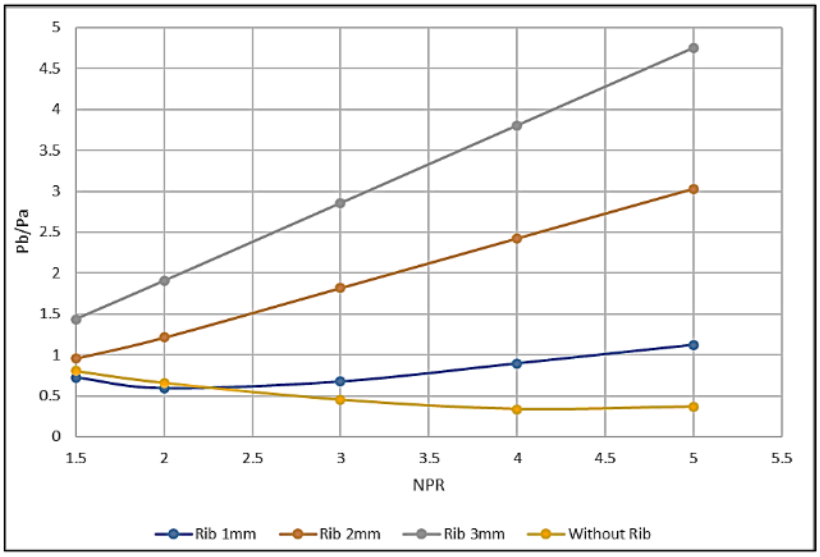
Pb/Pa
NPR
Rib 1mm
Rib 2mm
Rib 3mm
Without Rib

(c)

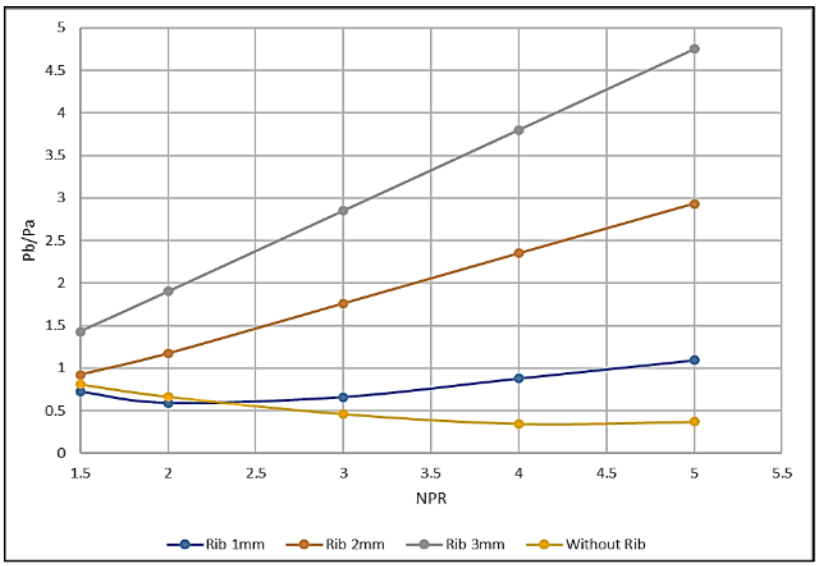
Pb/Pa
NPR
Rib 1mm
Rib 2mm
Rib 3mm
Without Rib

(d)

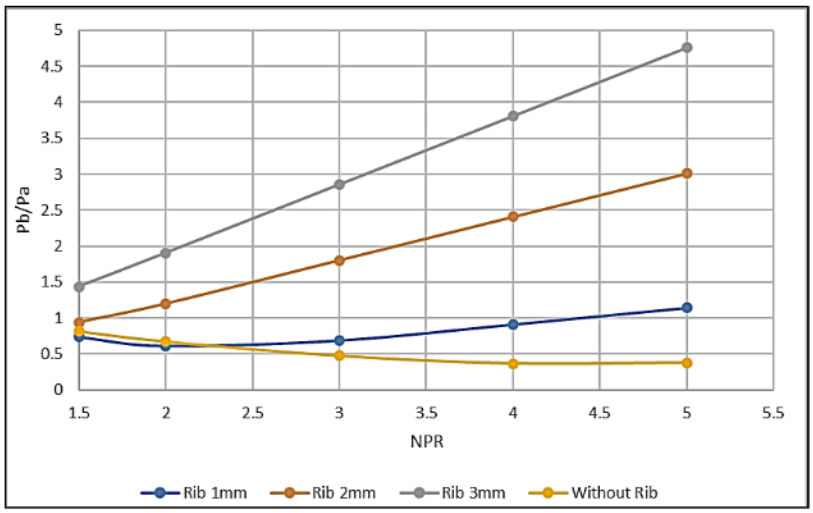

(e)

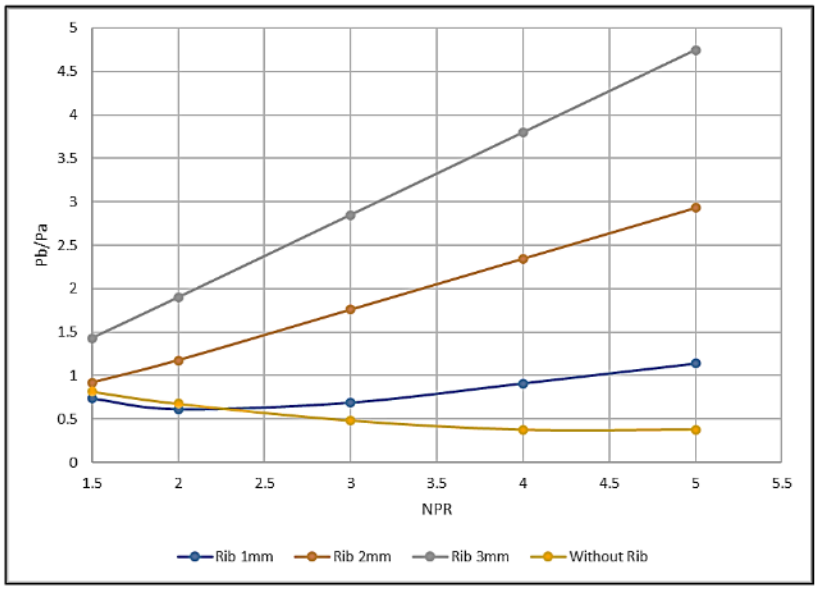

(f)

Fig. 12. Base pressure variation with NPR at rib location at 0.5D for various duct sizes and rib orientation 2 (a) L/D = 1 (b) L/D = 2 (c) L/D = 3 (d) L/D = 4 (e) L/D = 5 (f) L/D = 6

4.2.2 Base pressure results for rib located at 1D

When the rib is placed at a 1D location inside the duct, the base pressure with Nozzle Pressure Ratio is plotted for various duct lengths as shown in Figures 13(a) to 13(e). With a further shift of the rib location towards the downstream at 1D, there is a significant change in the base pressure pattern. Figures 13(a) shows that even for a 1 mm rib, the decreasing trend is controlled, and for NPR = 5, the base pressure is forty percent more than the atmospheric pressure. For a 2 mm rib, the initial base pressure value is nearly the atmospheric pressure value, and at NPR = 5, it attains a base pressure ratio of 3.5. Similar results are seen for the remaining duct lengths L/D = 3, 4, 5, and 6, as seen in Figures 13(b) to 13(d), with marginal variations in the base pressure data. These changes were expected due to the modification in duct size and the influence of the ambient atmospheric pressure.

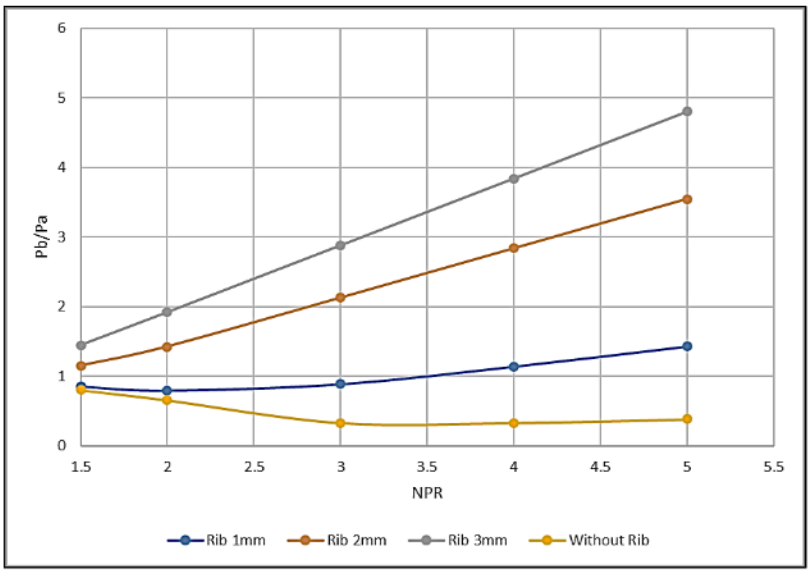
Pb/Pa
NPR
Rib 1mm
Rib 2mm
Rib 3mm
Without Rib

(a)

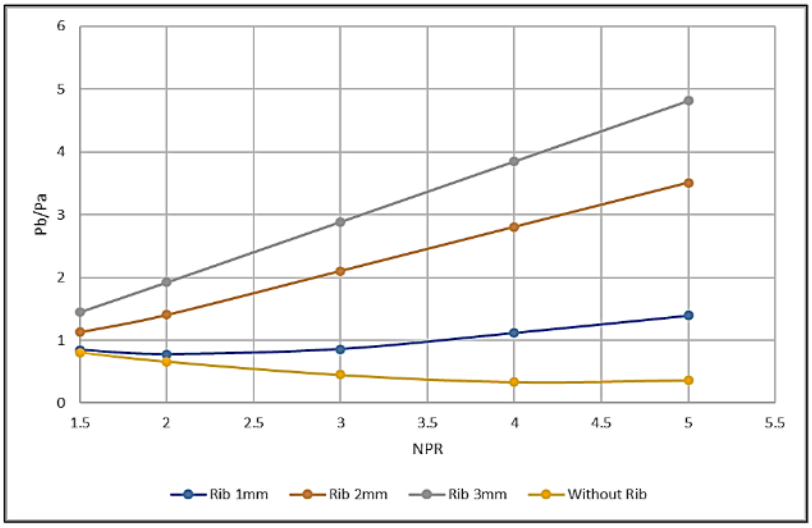
Pb/Pa
NPR
Rib 1mm
Rib 2mm
Rib 3mm
Without Rib

(b)

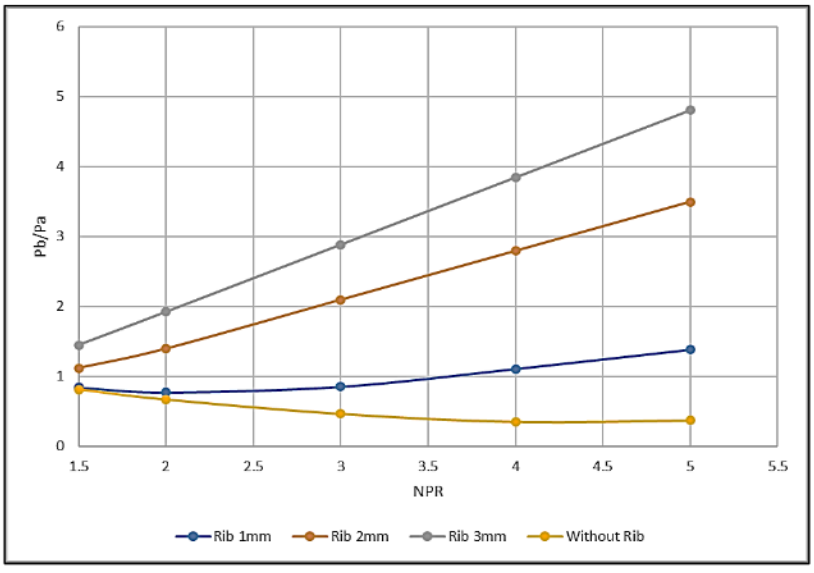
Pb/Pa
NPR
Rib 1mm
Rib 2mm
Rib 3mm
Without Rib

(c)

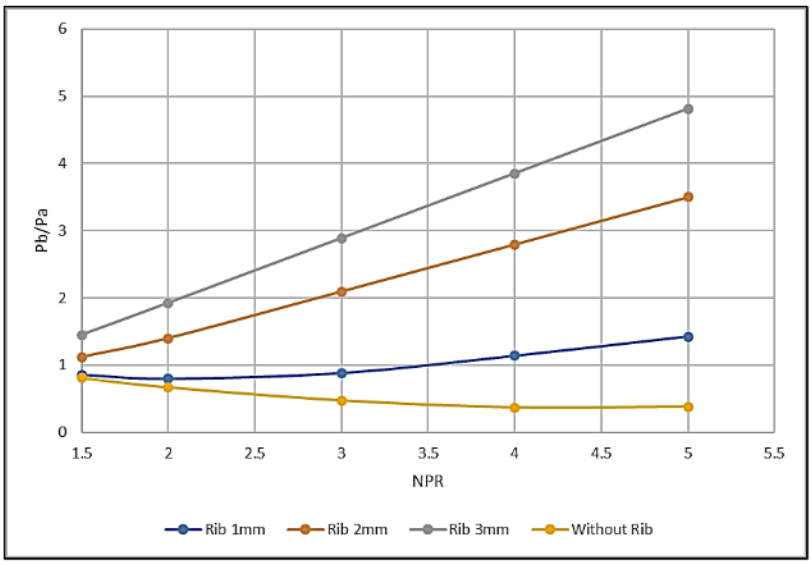

(d)

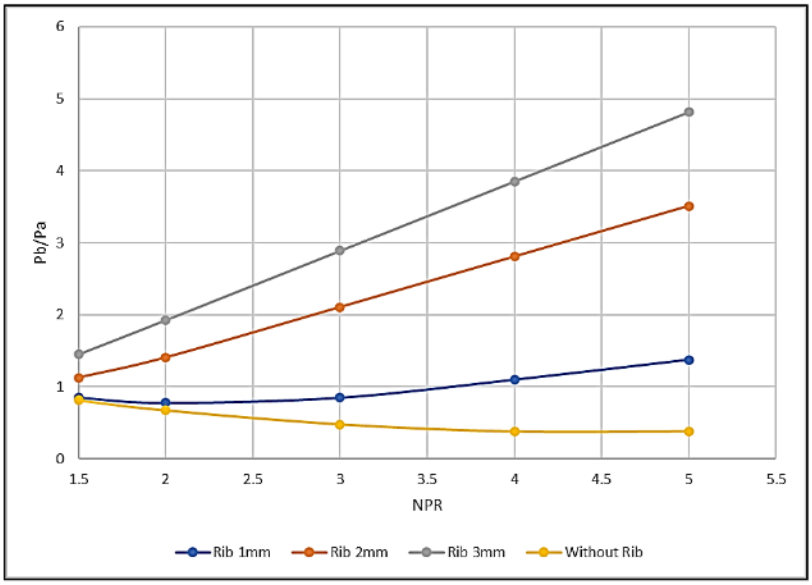

(e)

Fig. 13. Base pressure variation with NPR at rib location at 1D for various duct sizes and rib orientation 2 (a) L/D = 2 (b) L/D = 3 (c) L/D = 4 (d) L/D = 5 (e) L/D = 6

4.2.3 Base pressure results for rib located at 1.5D

For rib location is 1.5D, the findings of this study are shown in Figures 14(a) to 14(e) for various nozzle pressure ratios and duct sizes. Figure 14(a) shows the results for duct L/D = 2. The figure shows that as far as the 3 mm rib is concerned, there is no change in its value. Meanwhile, for rib radii 1 mm and 2 mm, there is a slight increase in the base pressure values. Similar results are seen for other duct lengths, namely L/D = 3, 4, 5, and 6, with slight changes in their values because of changes in duct lengths and the influence of the atmospheric pressure.

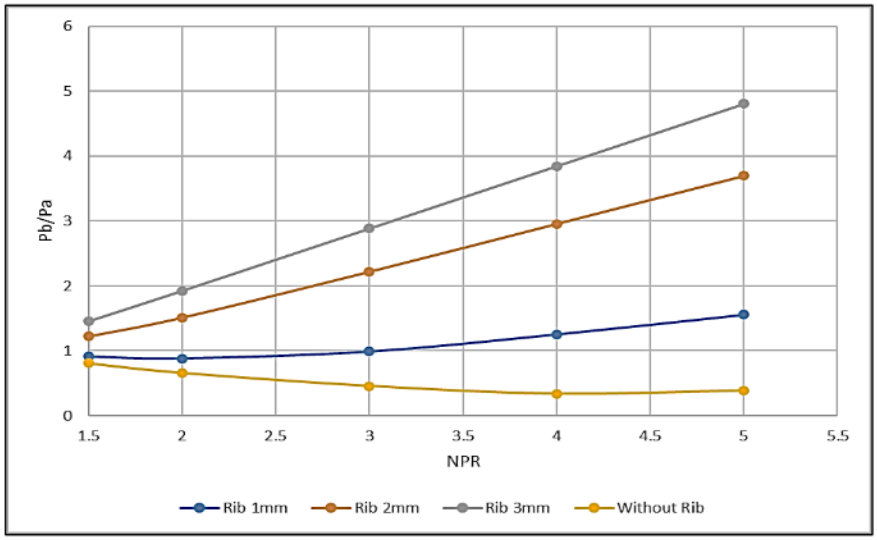
Pb/Pa
NPR
Rib 1mm
Rib 2mm
Rib 3mm
Without Rib

(a)

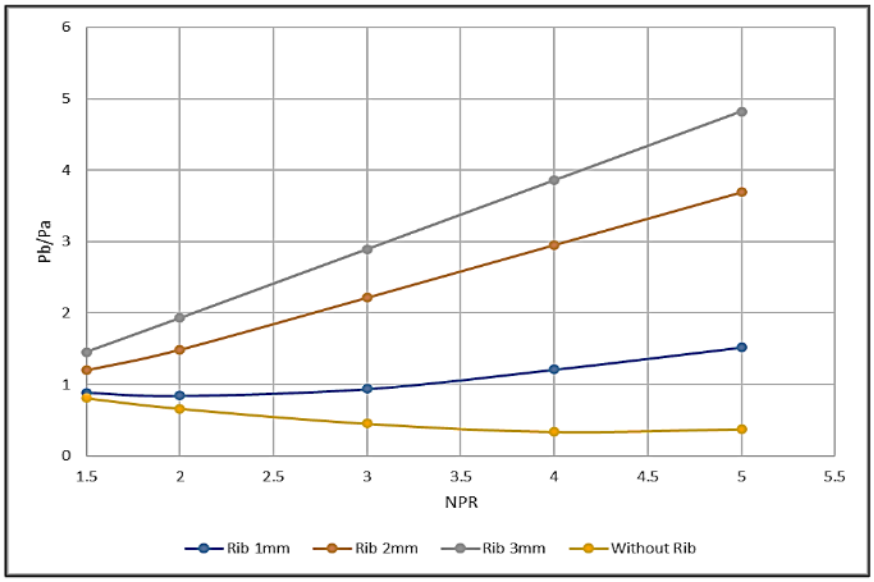
Pb/Pa
NPR
Rib 1mm
Rib 2mm
Rib 3mm
Without Rib

(b)

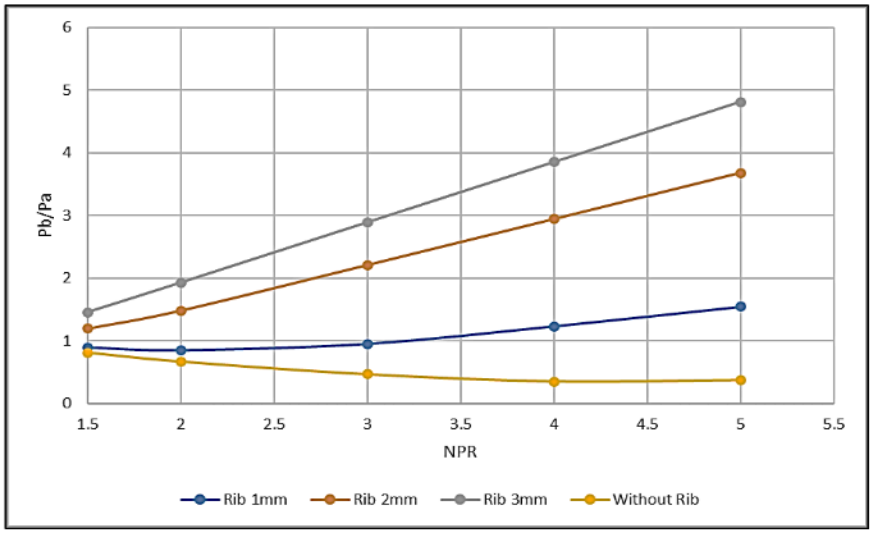
Pb/Pa
NPR
Rib 1mm
Rib 2mm
Rib 3mm
Without Rib

(c)

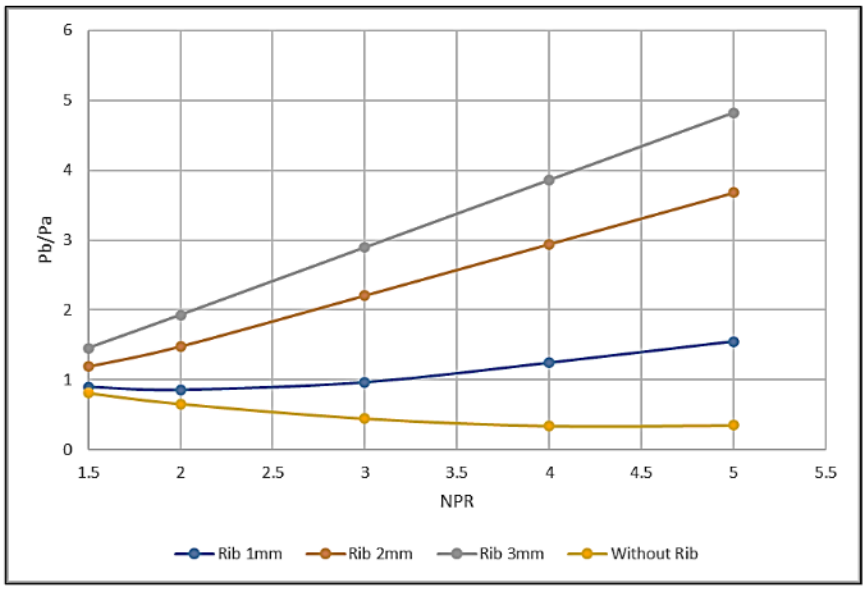

(d)

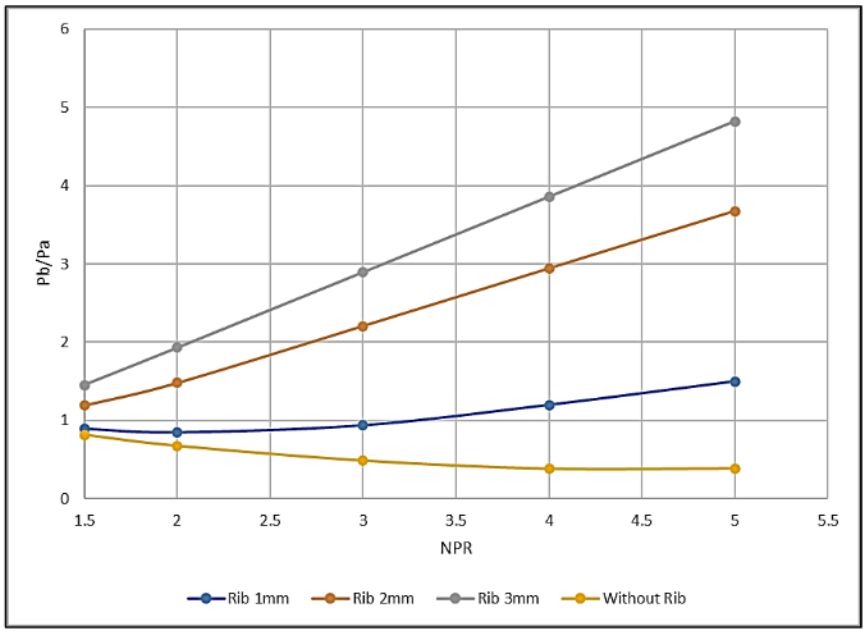

(e)

Fig. 14. Base pressure variation with NPR at rib location at L/D = 1.5 for various duct sizes and rib orientation 2 (a) L/D = 2 (b) L/D = 3 (c) L/D = 4 (d) L/D = 5 (e) L/D = 6

4.2.4 Base pressure results for rib located at 2D

For the Rib location, which is 2D, the base pressure results for various NPRs and duct sizes are shown in Figures 15(a) to (d). From Figures 15(a), it is seen that a further shift in the rib does not yield any significant change in the base pressure as the rib's location is beyond the reattachment point. As discussed earlier, any passive control location beyond the reattachment point will not result in any positive results, as the reattachment acts as an insulation point, and the flow cannot impact the separated recirculation base region. As discussed earlier, similar results for the other duct lengths are shown in Figures 15(b) to 15(d). However, small fluctuations are seen in the base pressure values

due to the changes in the duct length-to-diameter ratio and the influence of the atmospheric pressure.

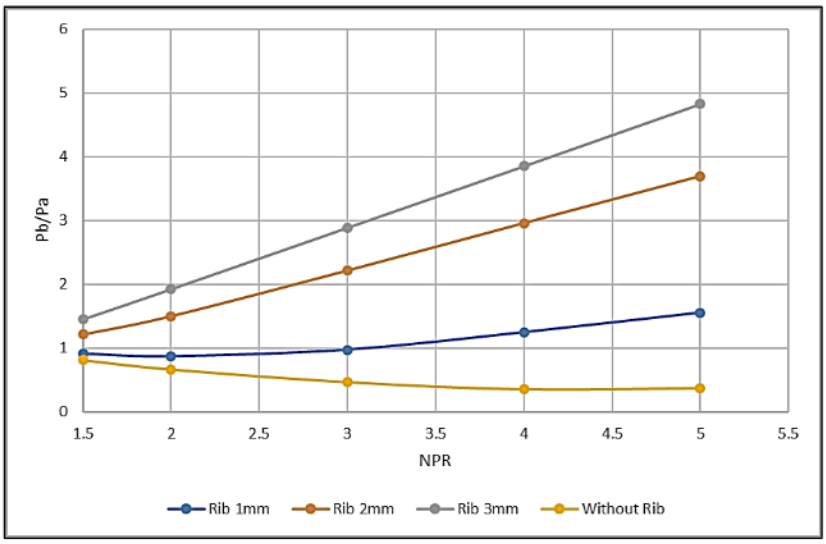

(a)

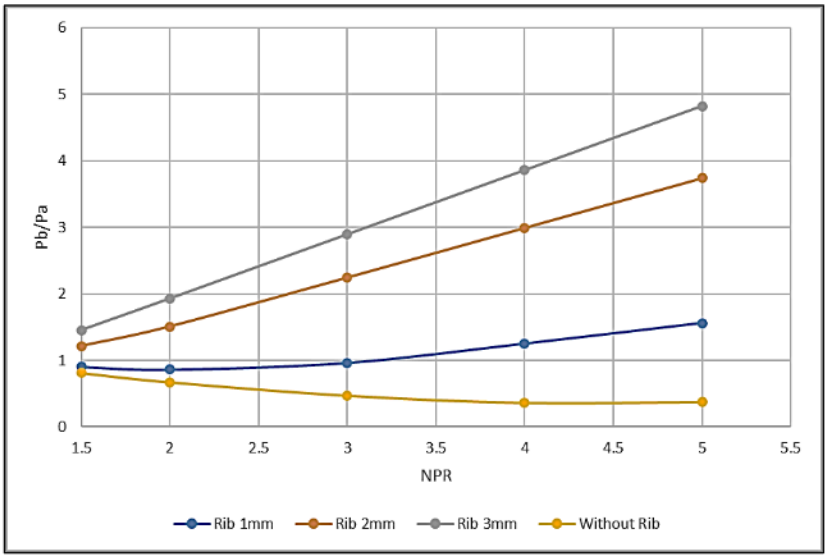

(b)

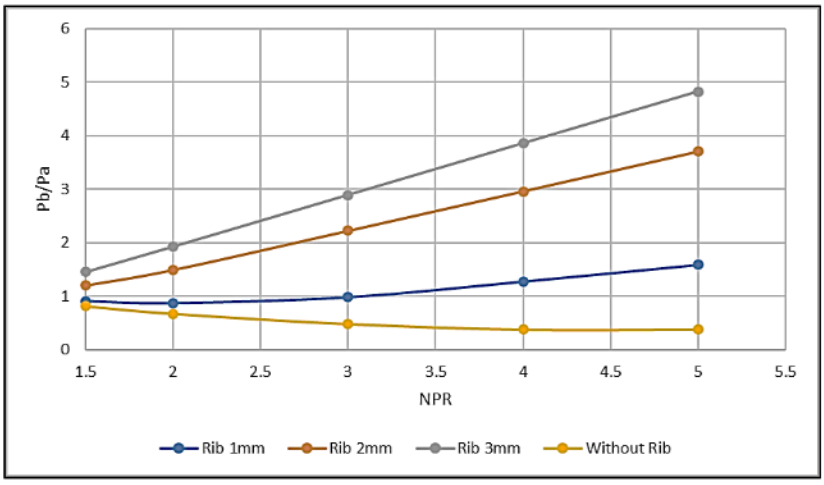

(c)

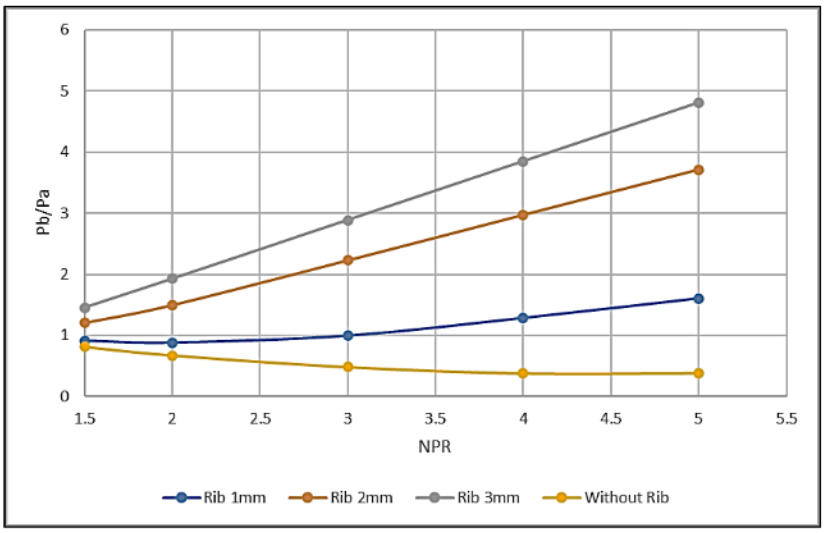

(d)

Fig. 15. Base pressure variation with NPR at rib location 2D for various duct sizes and rib orientation 2 (a) L/D = 3 (b) L/D = 4 (c) L/D = 5 (d) L/D = 6

4.2.5 Base pressure results for rib location at L/D = 3.0

When the rib is further shifted, the downstream outcomes of this study are shown in Figures 16(a) to 16(c). The duct diameter is 18 mm, and the reattachment point is expected to be around L/D = 1 or L/D = 1.5. As the rib location is far from the reattachment point, as expected, any shift in the rib location beyond 1.5D will not yield any beneficial results. The magnitude of the base pressure results in Figures 16(a) to 16(c) being the same as seen earlier.

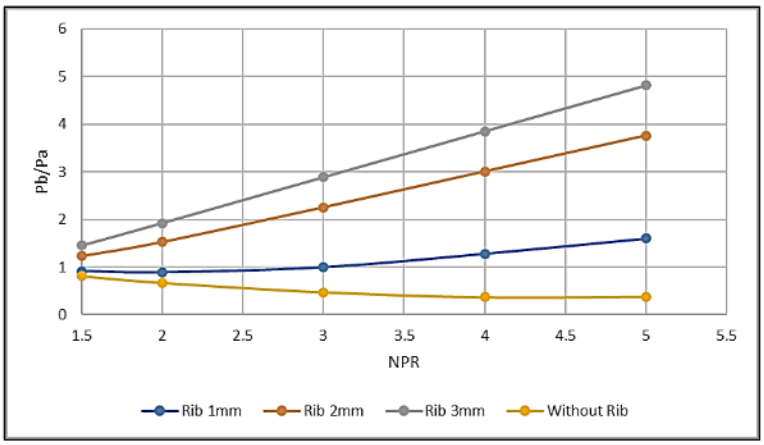

(a)

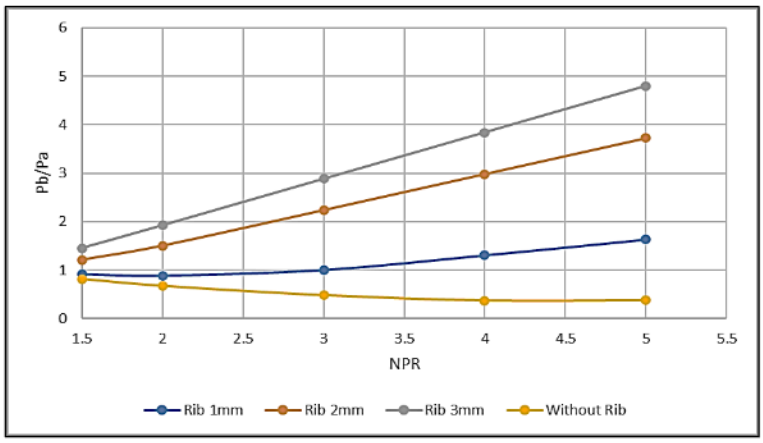

(b)

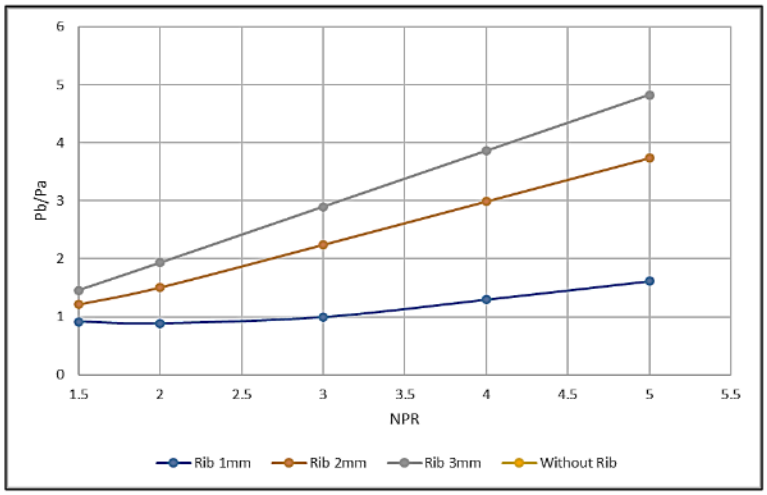

(c)

Fig. 16. Base pressure variation with NPR at rib location 3D for various duct sizes and rib orientation 2 (a) L/D = 4 (b) L/D = 5 (c) L/D = 6

4.3 Pressure and Velocity Contours for Rib Orientation 1

Figures 17(a) 17(e) shows the pressure contours for various rib locations at L/D= 4, NPR = 3, rib diameter = 2 mm, and rib orientation 1. From the pressure contour plots, it can be seen that the rib is effective for increasing the base pressure.

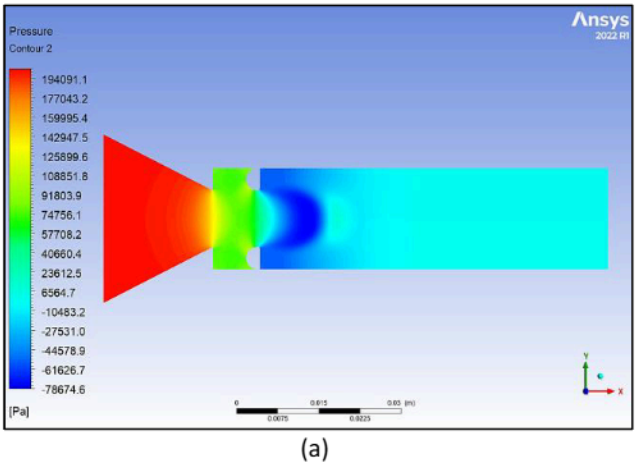

(a)

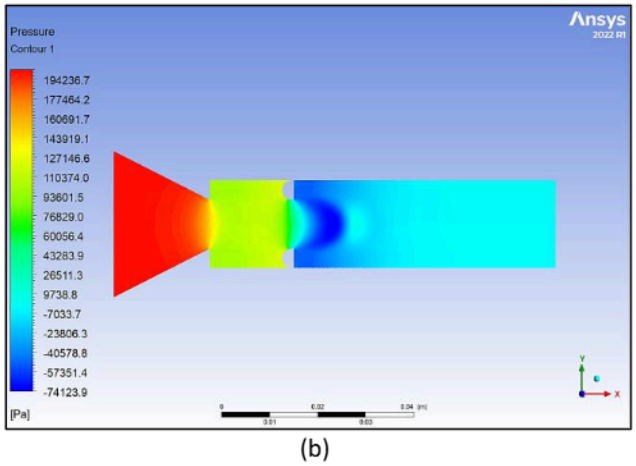

(b)

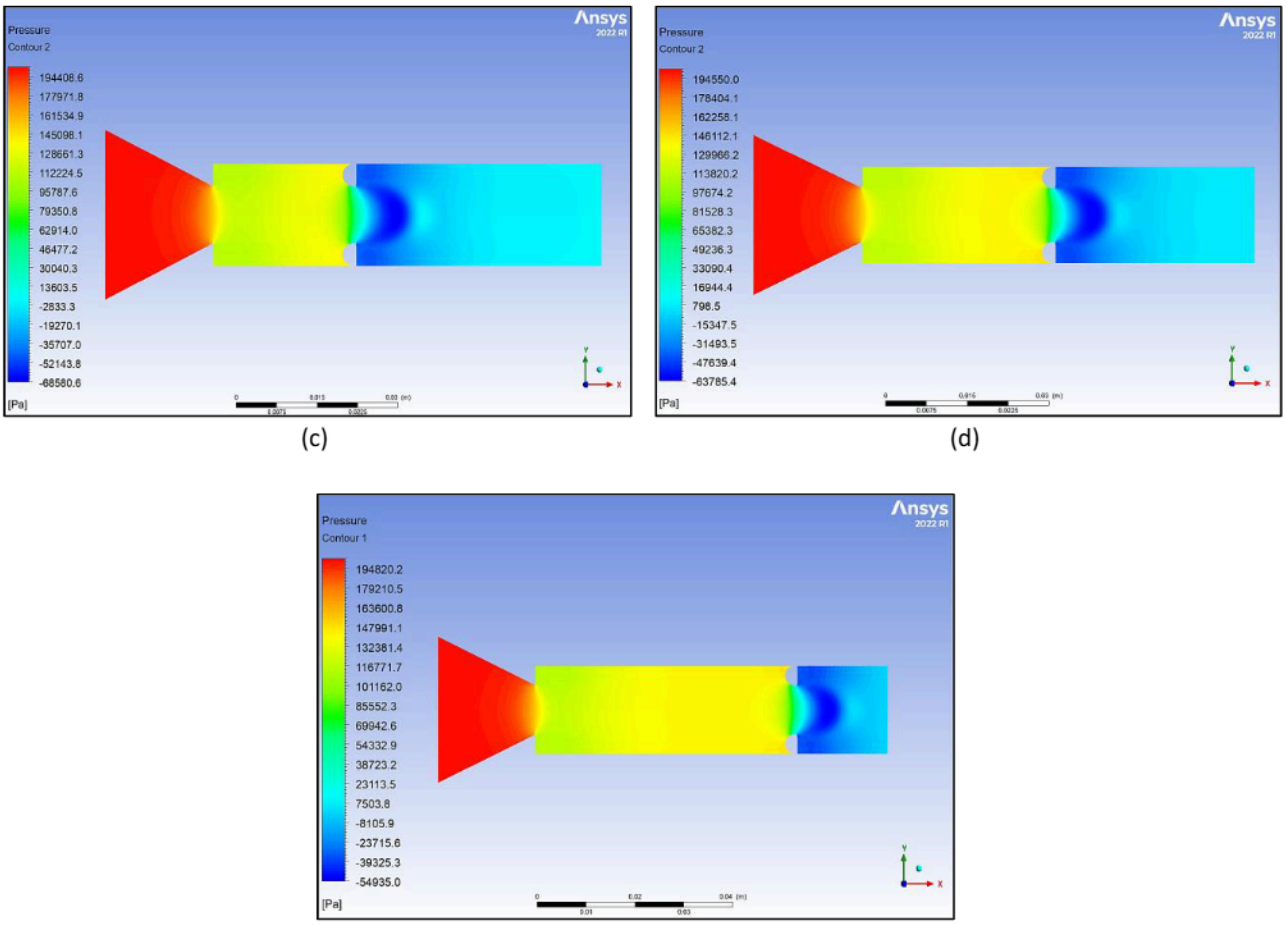

Fig. 17. Pressure contours for various locations of rib at L/D = 4, NPR = 3, rib diameter = 2 mm and rib orientation 1 (a) 0.5D (b) 1D (c) 1.5D (d) 2D (e) 3D

Figures 18(a) to 18(e) shows the velocity contours for various rib locations at L/D = 4, NPR = 3, rib diameter = 2 mm, and rib orientation 1. From the velocity contour plots, it can be seen that the rib is effective in increasing the base pressure.

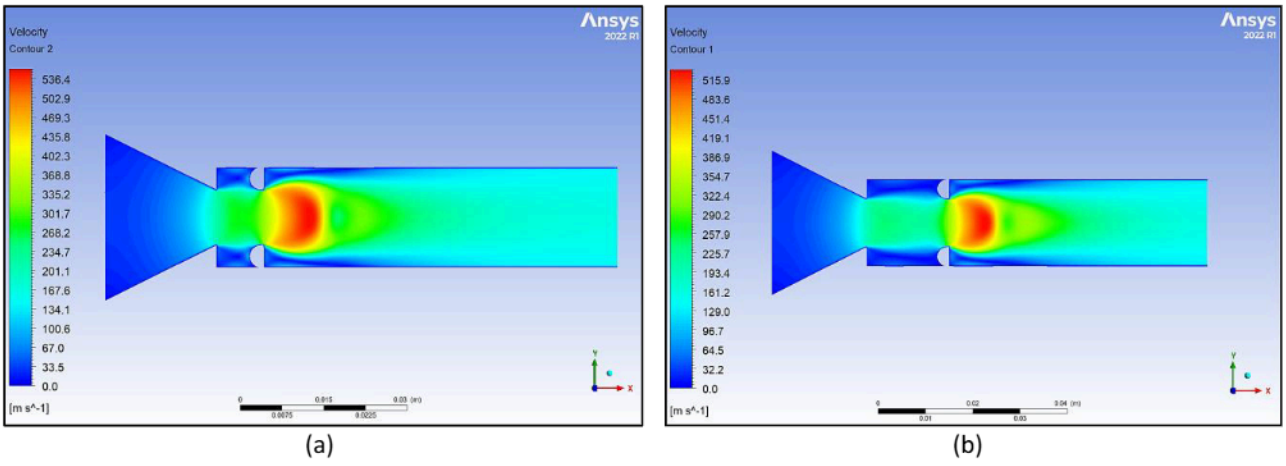

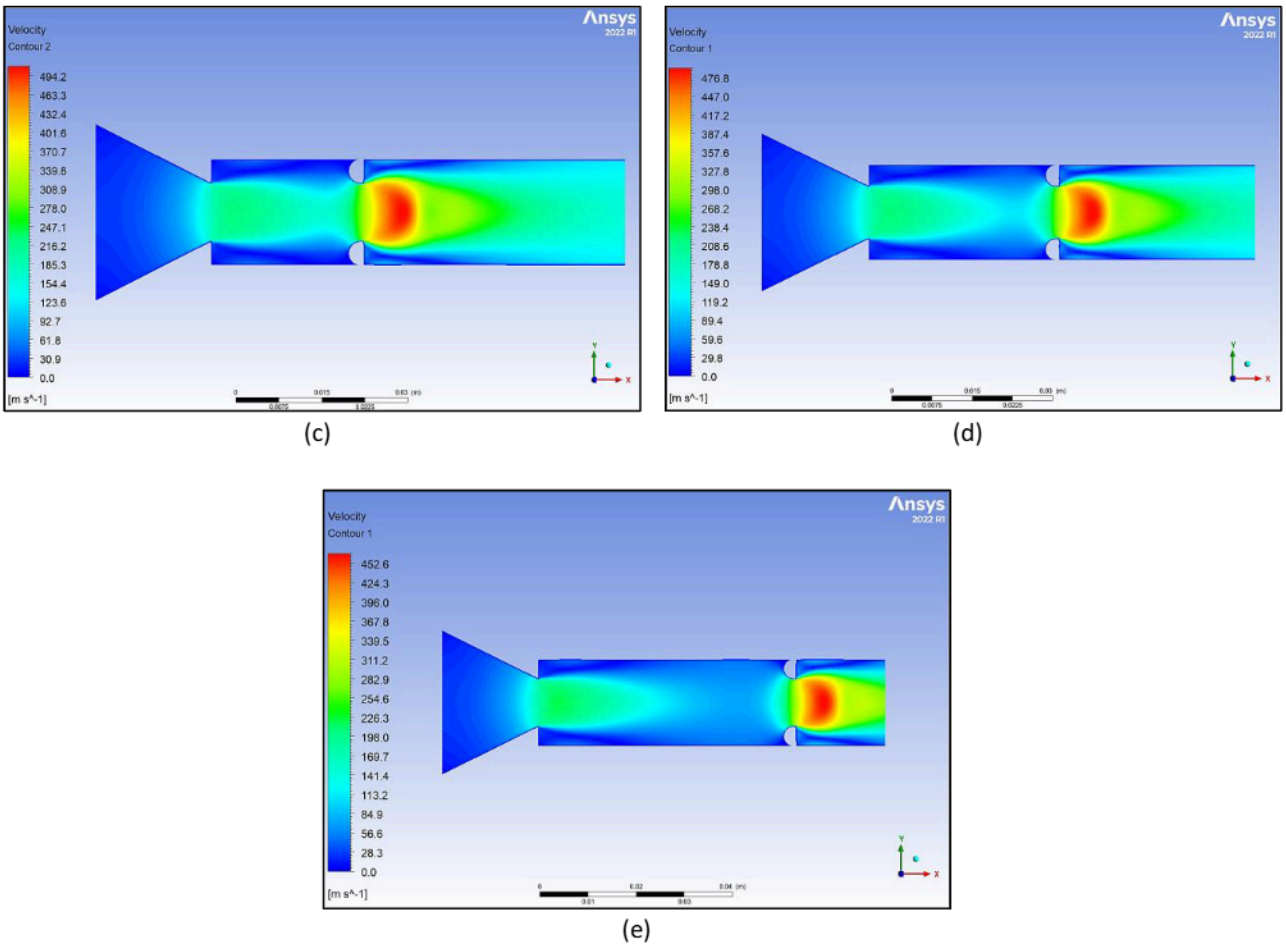

Fig. 18. Velocity contours for various locations of rib at L/D = 4, NPR = 3, rib diameter = 2 mm, and rib orientation 1 (a) 0.5D (b) 1D (c) 1.5D (d) 2D (e) 3D

5. Conclusions

The following conclusions may be drawn based on the above discussions. CFD simulations were done for orientations one and two for rib radii 1 mm, 2 mm, and 3 mm for duct L/D ratios 1, 2, 3, 4, 5, and 6. When the rib had orientation 1, the effectiveness of a 1 mm rib was less than that of orientation 2 of the rib. When the rib has orientation 2, and the shear layer faces the straight part of the rib, the base pressure's magnitude is higher than orientation 1. There is a progressive increase in the base pressure for rib location 0.5D to 1.5D. A further shift in the rib location downstream does not result in any increase in the base pressure. It is due to the position of the reattachment point, as any position of the rib beyond the reattachment point cannot influence the flow in the base region.

It is seen that with a 1 mm rib as a control mechanism, the base pressure attains a value more than ambient pressure. Hence, if the user must equate the base pressure with atmospheric pressure, then a 1 mm rib radius at the 1D location is the right choice. If it is required to raise the base pressure by a considerable value, then higher values of rib radius are to be considered. For fixed rib locations, the base pressure values remained almost the same, even though the duct lengths varied from L/D = 1 to 6. However, a slight variation in the base pressure is observed due to the combined effect of the duct length and the influence of the ambient atmosphere pressure.

References

[1] Khan, Sher Afghan, M. A. Fatepurwala, and K. N. Pathan. "CFD analysis of human powered submarine to minimize drag." *International Journal of Mechanical and Production* 8, no. 3 (2018). https://doi.org/10.24247/ijmperdjun2018111

[2] Pathan, Khizar A., Sher A. Khan, N. A. Shaikh, Arsalan A. Pathan, and Shahnawaz A. Khan. "An investigation of boattail helmet to reduce drag." *Advances in Aircraft and Spacecraft Science* 8, no. 3 (2021): 239. https://doi.org/10.12989/aas.2021.8.3.239

[3] Pathan, Khizar Ahmed, Syed Ashfaq, Prakash S. Dabeer, and Sher Afgan Khan. "Analysis of parameters affecting thrust and base pressure in suddenly expanded flow from nozzle." *Journal of Advanced Research in Fluid Mechanics and Thermal Sciences* 64, no. 1 (2019): 1-18.

[4] Pathan, Khizar A., Prakash S. Dabeer, and Sher A. Khan. "Enlarge duct length optimization for suddenly expanded flows." *Advances in Aircraft and Spacecraft Science* 7, no. 3 (2020): 203-214. https://doi.org/10.12989/aas.2020.7.3.203

[5] Pathan, Khizar Ahmed, Prakash S. Dabeer, and Sher Afghan Khan. "Influence of expansion level on base pressure and reattachment length." *CFD Letters* 11, no. 5 (2019): 22-36.

[6] Pathan, Khizar Ahmed, Zakir Ilahi Chaudhary, Ajaj Rashid Attar, Sher Afghan Khan, and Ambareen Khan. "Optimization of nozzle design for weight reduction using variable wall thickness." *Journal of Advanced Research in Fluid Mechanics and Thermal Sciences* 112, no. 2 (2023): 86-101. https://doi.org/10.37934/arfmts.112.2.86101

[7] Fakhruddin, Ahmad'Afy Ahmad, Fharukh Ahmed Ghasi Mahaboobali, Ambareen Khan, Mohammad Nishat Akhtar, Sher Afghan Khan, and Khizar Ahmad Pathan. "Analysis of base pressure control with ribs at Mach 1.2 using cfd method." *Journal of Advanced Research in Fluid Mechanics and Thermal Sciences* 123: 108-143. https://doi.org/10.37934/arfmts.123.1.108143

[8] Khan, Ambareen, Parvathy Rajendran, Junior Sarjit Singh Sidhu, and Mohsen Sharifpur. "Experimental investigation of suddenly expanded flow at sonic and supersonic Mach numbers using semi-circular ribs: a comparative study between experimental, single layer, deep neural network (SLNN and DNN) models." *The European Physical Journal Plus* 138, no. 4 (2023): 314. https://doi.org/10.1140/epjp/s13360-023-03853-1

[9] Khan, Ambareen, Abdul Aabid, Sher Afghan Khan, Mohammad Nishat Akhtar, and Muneer Baig. "Comprehensive CFD analysis of base pressure control using quarter ribs in sudden expansion duct at sonic Mach numbers." *International Journal of Thermofluids* 24 (2024): 100908. https://doi.org/10.1016/j.ijft.2024.100908

[10] Khan, Ambareen, Sher Afghan Khan, Vijayanandh Raja, Abdul Aabid, and Muneer Baig. "Effect of ribs in a suddenly expanded flow at sonic Mach number." *Heliyon* 10, no. 9 (2024). https://doi.org/10.1016/j.heliyon.2024.e30313

[11] Khan, Ambareen, Sher Afghan Khan, Mohammed Nishat Akhtar, Abdul Aabid, and Muneer Baig. "Base pressure control with semi-circular ribs at critical Mach number." *Fluid Dynamics & Materials Processing* 20, no. 9 (2024). http://dx.doi.org/10.32604/fdmp.2024.049368

[12] Nurhanis, Tun, Ambareen Khan, Mohammad Nishat Akhtar, and Sher Afghan Khan. "Control of base pressure at supersonic Mach number in a suddenly expanded flow." *Journal of Advanced Research in Fluid Mechanics and Thermal Sciences* 109 (2023): 210-225. https://doi.org/10.37934/arfmts.109.1.210225

[13] Khan, Ambareen, Nurul Musfirah Mazlan, and Mohd Azmi Ismail. "Velocity distribution and base pressure analysis of under expanded nozzle flow at Mach 1.0." *Journal of Advanced Research in Fluid Mechanics and Thermal Sciences* 92: 177-189. https://doi.org/10.37934/arfmts.92.1.177189

[14] Khan, Ambareen, Nurul Musfirah Mazlan, and Ervin Sulaeman. "Effect of ribs as passive control on base pressure at sonic Mach numbers." *CFD Letters* 14 (2022): 140-151. https://doi.org/10.37934/cfdl.14.1.140151

[15] Khan, Ambareen, Mohd Azmi Ismail, and Nurul Musfirah Mazlan. "Numerical simulation of suddenly expanded flow from converging nozzle at sonic Mach number." In *Proceedings of International Conference of Aerospace and Mechanical Engineering 2019: AeroMech 2019, 20–21 November 2019, Universiti Sains Malaysia, Malaysia*, p. 349-359. Singapore: Springer Singapore, 2020. https://doi.org/10.1007/978-981-15-4756-0_29

[16] Chaudhary, Zakir Ilahi, Ambareen Khan, Sher Afghan Khan, and Khizar Ahmed Pathan. "Base pressure control using quarter circle rib in a suddenly expanded duct at screech prone Mach number M= 1.8." *CFD Letters* 17, no. 8 (2025): 60-95. https://doi.org/10.37934/cfdl.17.8.6095

[17] Bellary, Sayed Ahmed Imran, Ambareen Khan, Mohammad Nishat Akhtar, Dabir Shahab, Sher Afghan Khan, and Khizar Ahmed Pathan. "Numerical simulations of base pressure and its control in a suddenly expanded duct at Mach 1.6 using quarter circular ribs." *Journal of Advanced Research in Fluid Mechanics and Thermal Sciences* 127, no. 2 (2025): 203-233. https://doi.org/10.37934/arfmts.127.2.203233

[18] Shetty, Shamitha, Fharukh Ahmed Ghasi Mahaboobali, Ambareen Khan, Mohmmad Nishat, Sher Afghan Khan Akhtar, and Khizar Ahmed Pathan. "Base pressure control using quarter rib at Mach 1.3: A comprehensive CFD

analysis."*Journal of Advanced Research in Fluid Mechanics and Thermal Sciences* 127, no. 2 (2025): 1-32. https://doi.org/10.37934/arfmts.127.2.132

[19] Mahaboobali, Fharukh Ahmed Ghasi, Ambareen Khan, Mohammad Nishat Akhtar, S. A. Khan, and K. A. Pathan. "Passive control of base flows and impact of quarter rib radius and locations at Sonic Mach number."*Journal of Advanced Research in Numerical Heat Transfer* 30, no. 1 (2025): 47-81. https://doi.org/10.37934/arnht.30.1.4781

[20] Sajali, Muhammad Fahmi Mohd, Abdul Aabid, Sher Afghan Khan, Fharukh Ahmed Ghasi Mehaboobali, and Erwin Sulaeman. "Numerical investigation of flow field of a non-circular cylinder."*CFD Letters* 11, no. 5 (2019): 37-49.

[21] Khan, Sher Afghan, Mohammed Asadullah, and Jafar Sadhiq. "Passive control of base drag employing dimple in subsonic suddenly expanded flow." *International Journal of Mechanical and Mechatronics Engineering* 18, no. 3 (2018): 69-74. https://doi.org/10.1108/00022660810859373

[22] Fiqri, Muhammad Ikhwan, Khizar Ahmed Pathan, and Sher Afghan Khan. "Control of suddenly expanded flow with cavity at Sonic Mach number." In *International Conference on Advances in Heat Transfer and Fluid Dynamics*, p. 3-15. Singapore: Springer Nature Singapore, 2022. https://doi.org/10.1007/978-981-99-7213-5_1

[23] Aqilah, Nur, Khizar Ahmed Pathan, and Sher Afghan Khan. "Passive control of base flow at supersonic Mach number for area ratio 4." In *International Conference on Advances in heat Transfer and Fluid Dynamics*, p. 37-50. Singapore: Springer Nature Singapore, 2022. https://doi.org/10.1007/978-981-99-7213-5_4

[24] Azami, Muhammed Hanafi, Mohammed Faheem, Abdul Aabid, Imran Mokashi, and Sher Afghan Khan. "Inspection of supersonic flows in a CD nozzle using experimental method." *International Journal of Recent Technology and Engineering* 8, no. 2S3 (2019): 996-999. https://doi.org/10.35940/ijrte.B1186.0782S319

[25] Khan, Sher Afghan, and Ethirajan Rathakrishnan. "Active control of suddenly expanded flows from underexpanded nozzles." *International Journal of Turbo and Jet Engines* 21, no. 4 (2004): 233-254. https://doi.org/10.1515/TJJ.2005.22.3.163

[26] Rehman, Shafiqur, and Sher Afghan Khan. "Control of base pressure with micro-jets: part I." *Aircraft Engineering and Aerospace Technology* 80, no. 2 (2008): 158-164. https://doi.org/10.1108/00022660810859373

[27] Shaikh, Javed S., Krishna Kumar, Khizar A. Pathan, and Sher A. Khan. "Analytical and computational analysis of pressure at the nose of a 2D wedge in high speed flow." *Advances in Aircraft and Spacecraft Science* 9, no. 2 (2022): 119-130.

[28] Shamitha, Asha Crasta, Khizar Ahmed Pathan, and Sher Afghan Khan. "Numerical simulation of surface pressure of a wedge at supersonic Mach numbers and application of design of experiments." *Journal of Advanced Research in Applied Mechanics* 101 no. 1 (2023): 1-18. https://doi.org/10.37934/aram.101.1.118

[29] Shamitha, Shamitha, Khizar Ahmed Pathan, and Sher Afghan Khan. "Analytical and numerical simulation of surface pressure of an oscillating wedge at hypersonic Mach numbers and application of Taguchi's method." *Journal of Advanced Research in Applied Sciences and Engineering Technology* 30, no. 1 (2023): 15-30. https://doi.org/10.37934/araset.30.1.1530

[30] Shaikh, Javed Shoukat, Khizar Ahmed Pathan, Krishna Kumar, and Sher Afghan Khan. "Effectiveness of cone angle on surface pressure distribution along slant length of a cone at hypersonic Mach numbers." *Journal of Advanced Research in Fluid Mechanics and Thermal Sciences* 104, no. 1 (2023): 185-203. https://doi.org/10.37934/arfmts.104.1.185203

[31] Shaikh, Javed Shoukat, Khizar Ahmed Pathan, Krishna Kumar, and Sher Afghan Khan. "Effectiveness of cone angle on surface pressure distribution along slant length of a cone at hypersonic Mach numbers." *Journal of Advanced Research in Fluid Mechanics and Thermal Sciences* 104, no. 1 (2023): 185-203. https://doi.org/10.32604/fdmp.2023.025113

[32] Shaikh, Javed Shoukat, Khizar Ahmed Pathan, and Sher Afghan Khan. "Numerical simulation of surface pressure and temperature distribution along a cone at supersonic Mach numbers using CFD." *Journal of Advanced Research in Numerical Heat Transfer* 28, no. 1 (2025): 1-26. https://doi.org/10.37934/arnht.28.1.126

[33] Shaikh, Javed Shoukat, Krishna Kumar, Khizar Ahmed Pathan, Sher Afghan Khan, Fayaz Husain Kharadi, and Afreen Siddiqui. "Estimation of the damping derivative in pitch for a wedge at supersonic Mach numbers using design of experiments." *Journal of Advanced Research in Experimental Fluid Mechanics and Heat Transfer* 18, no. 1 (2025): 106-117. https://doi.org/10.37934/arfmts.18.1.106117

[34] Shaikh, Javed Shoukat, Shamitha Shetty, Khizar Ahmed Pathan, Narayan Govindrao Abuj, Krishna Kumar, Sher Afgan Khan, and Anurag A. Nema. "Numerical modeling and analysis of damping derivatives for a 2D wedge at hypersonic mach numbers and variable pivot points." *Journal of Advanced Research in Fluid Mechanics and Thermal Sciences* 128, no. 1 (2025): 92-107. https://doi.org/10.37934/arfmts.128.1.92107

[35] Khalil, Shaikh Sohel Mohd, Rai Sujit Nath Sahai, Nitin Parashram Gulhane, Khizar Ahmed Pathan, Ajaj Rashid Attar, and Sher Afghan Khan. "Experimental investigation of local nusselt profile dissemination to augment heat transfer under air jet infringements for industrial applications." *Journal of Advanced Research in Fluid Mechanics and Thermal Sciences* 112: 161-173. https://doi.org/10.37934/arfmts.112.2.161173

[36] Shaikh, Sohel Khalil, Khizar Ahmed Pathan, Zakir Ilahi Chaudhary, B. G. Marlpalle, and Sher Afghan Khan. "An investigation of three-way catalytic converter for various inlet cone angles using CFD." *CFD Letters* 12, no. 9 (2020): 76-90. https://doi.org/10.37934/cfdl.12.9.7690

[37] Shaikh, Sohel Khalil, Khizar Ahmed Pathan, Zakir Ilahi Chaudhary, and Sher Afghan Khan. "CFD analysis of an automobile catalytic converter to obtain flow uniformity and to minimize pressure drop across the monolith." *CFD Letters* 12, no. 9 (2020): 116-128. https://doi.org/10.37934/cfdl.12.9.116128

[38] Khan, Sher Afghan, and Ethirajan Rathakrishnan. "Nozzle expansion level effect on suddenly expanded flow." *International Journal of Turbo and Jet Engines* 23, no. 4 (2006): 233-258. https://doi.org/10.1515/TJJ.2006.23.4.233

[39] Aabid, Abdul, Ambareen khan, Nurul Musfirah. Mazlan, Mohd Azmi. Ismail, Mohammad Nishat Akhtar, and S. A. Khan. "Numerical simulation of suddenly expanded flow at Mach 2.2." *International Journal of Engineering and Advanced Technology* 8, no. 3 (2019): 457-462.

[40] Baig, Maughal Ahmed Ali, Fahad Al-Mufadi, Sher Afghan Khan, and Ethirajan Rathakrishnan. "Control of base flows with micro jets." *International Journal of Turbo and Jet Engines* 28, no. 1 (2011): 59-69. https://doi.org/10.1515/tjj.2011.009

[41] Chaudhary, Zakir Ilahi, Ambareen Khan, Sher Afghan Khan, Mohammad Nishat Akhtar, and Khizar Ahmed Pathan. "Control of suddenly expanded flow using quarter rib for area ratio 4.84 at Mach 2." *Journal of Advanced Research in Experimental Fluid Mechanics and Heat Transfer* 19, no. 1 (2025): 1-29. https://doi.org/10.37934/arfmts.19.1.129

[42] Rathakrishnan, E. "Effect of ribs on suddenly expanded flows." *AIAA Journal* 39, no. 7 (2001): 1402-1404. https://doi.org/10.2514/2.1447